MOX-Report No. 03/2018

Fast numerical integration on polytopic meshes with applications to discontinuous Galerkin finite element methods

Antonietti, P. F.; Houston, P.; Pennesi, G.

MOX, Dipartimento di Matematica
Politecnico di Milano, Via Bonardi 9 - 20133 Milano (Italy)

mox-dmat@polimi.it http://mox.polimi.it

Fast numerical integration on polytopic meshes with applications to discontinuous Galerkin finite element methods*

Paola F. Antonietti[♮], Paul Houston[♭], Giorgio Pennesi[♮]

January 13, 2018

[♮] MOX-Laboratory for Modeling and Scientific Computing, Dipartimento di Matematica, Politecnico di Milano, Piazza Leondardo da Vinci 32, 20133 Milano, Italy.
paola.antonietti@polimi.it, giorgio.pennesi@polimi.it

[♭] School of Mathematical Sciences, University of Nottingham, University Park, Nottingham, NG7 2RD, UK.
paul.houston@nottingham.ac.uk

Abstract

In this paper we present efficient quadrature rules for the numerical approximation of integrals of polynomial functions over general polygonal/polyhedral elements that do not require an explicit construction of a sub-tessellation into triangular/tetrahedral elements. The method is based on successive application of Stokes' theorem; thereby, the underlying integral may be evaluated using only the values of the integrand at the vertices of the polytopic domain, and hence leads to an exact cubature rule whose quadrature points are the vertices of the polytope. We demonstrate the capabilities of the proposed approach by efficiently computing the stiffness and mass matrices arising from *hp*-version symmetric interior penalty discontinuous Galerkin discretizations of second-order elliptic partial differential equations.

1 Introduction

In recent years the exploitation of computational meshes composed of polygonal and polyhedral elements has become very popular in the field of numerical methods for partial differential equations. Indeed, the flexibility offered by polygonal/polyhedral elements allows for the design of efficient computational grids when the underlying problem is characterized by a strong complexity of the physical domain, such as, for example, in geophysical applications, fluid-structure interaction, or crack propagation problems. Moreover, the possibility to adopt computational meshes with hanging nodes is included in this framework by observing that, for example, a classical quadrilateral element with a hanging node on one of its edges can be treated as a pentagon with two aligned edges. Several conforming numerical discretization methods which admit polygonal/polyhedral meshes have been proposed within the current literature; here, we mention, for example,

*Paola F. Antonietti and Giorgio Pennesi have been partially funded by by the SIR Project n. RBSI14VT0S: "*PolyPDEs: Non-conforming polyhedral finite element methods for approximation of partial differential equations*" funded by MIUR - Italian Ministry of Education, Universities and Research - and by Fondazione Cariplo and Regione Lombardia research grant n. 2015-0182: "*PolyNuM: Polyhedral numerical methods for PDEs*".

the Composite Finite Element Method [41, 40, 7], the Mimetic Finite Difference (MFD) method [43, 20, 18, 19, 17, 6], the Polygonal Finite Element Method [60], the Extended Finite Element Method [61, 36], the Virtual Element Method (VEM) [14, 15, 16, 3, 4] and the Hybrid High-Order (HHO) method [34, 32, 33]. In the non-conforming setting, we mention Discontinuous Galerkin (DG) methods [1, 8, 24, 13, 21, 24, 22, 2, 5, 10, 23], Hybridizable DG methods [28, 29, 30, 31], the Non-conforming VEM [9, 12, 25], and the Gradient Schemes [35]; here the possibility of defining local polynomial discrete spaces follows naturally with the flexibility provided by polytopic meshes.

One of the key aspects concerning the development of efficient finite element discretizations with polygonal/polyhedral grids is the construction of quadrature formulae for the approximate computation of the terms appearing in the underlying weak formulation. Indeed, the design of efficient quadrature rules for the numerical computation of integrals over general shaped polytopes is far from being a trivial task. The classical and most widely employed technique for the integration over polytopes is the *Sub-Tessellation* method, cf. [50, 59, 37]; here, the domain of integration is subdivided into standard-shaped elements, such as triangular/quadrilateral elements in 2D or tetrahedral/hexahedral elements in 3D, whereby standard Gaussian quadrature rules are employed, cf. [57, 49, 67], and also [68] and [47], for an interpolation technique based on the same idea. On the one hand this technique is easy to implement, however, it is generally computationally expensive, particularly for high order polynomials, since the number of function evaluations may be very large.

For this reason, the development of quadrature rules that avoid sub-tessellation is an active research field. Several approaches have been proposed; in particular, we mention [64, 42, 65, 53], for example. One interesting method in this direction is represented by the *Moment fitting equation* technique, firstly proposed by Lyness and Monegato in [48], for the construction of quadrature rules on polygons featuring by the same symmetry as the regular hexagon. Generalization to convex and non-convex polygons and polyhedra was then proposed by Mousavi, Xiao and Sukumar in [52]. Here, starting from an initial quadrature rule, given, for example, by the sub-tessellation method described above, an iterative node elimination algorithm is performed based on employing the least-squares Newton's method [66] in order to minimise the number of quadrature points while retaining exact integration. Further improvements of the *Moment Fitting Equation* algorithm can also be found in [51] and [58]. While this method is optimal with respect to the number of function evaluations, the nodes and weights must be stored for every polygon, thus affecting memory efficiency. An alternative approach designed to overcome the limitations of the *Sub-Tessellation* approach is based on employing the generalized version of Stokes' theorem; here, the exploitation of Stokes' theorem reduces the integral over a polytope to an integration over its boundary; see [63] for details. For the two–dimensional case, in [56], Sommariva and Vianello proposed a quadrature rule based on employing Green's theorem. In particular, if an x- or y-primitive of the integrand is available (as for bivariate polynomial functions), the integral over the polygon is reduced to a sum of line integrations over its edges. When the primitive is not known, this method does not directly require a tessellation of the polygon, but a careful choice of the parameters related to the proposed formula leads to a cubature rule that can be viewed as a particular sub-tessellation of the polygon itself. Moreover, it is not possible to guarantee that all of the quadrature points lie inside the domain of integration. An alternative and very efficient formula has been proposed by Lasserre in [46] for the integration of *homogeneous functions* over convex polytopes. This technique has been recently extended to general convex and non-convex polytopes in [26]. The essential idea of this method is to exploit the generalized Stokes' theorem together with the Euler's homogeneous function theorem, cf. [55], in order to reduce the integration over a polytope only to boundary evaluations. The main difference with respect to the work presented in [56] is the possibility to apply the same idea recursively, leading to a quadrature formula which exactly evaluates integrals over a polygon/polyhedron by employing only point-evaluations of the integrand and its derivatives at the vertices of the polytope.

In this article we extend the approach of [26] to the efficient computation of the volume/face integral terms appearing in the discrete weak formulation of second-order elliptic problems, discretized by means of high-order DG methods. We point out that our approach is completely general and can be directly applied to other discretization schemes as VEM, HHO, Hybridisable DG, and MFD, for example. We focus on the DG approach presented in [24], where the local polynomial discrete spaces are defined based on employing the bounded box technique [38]. We show that our integration approach leads to a considerable improvement in the performance compared to classical quadrature algorithms based on sub-tessellation, in both two– and three–dimensions.

The rest of the paper is organized as follows: in Section 2 we recall the work introduced in [26], and outline how this approach can be utilized to efficiently compute the integral of d-variate polynomial functions over general polytopes. In Section 3 we introduce the interior penalty DG formulation for the numerical approximation of a second-order diffusion-reaction equation on general polytopic meshes. In Section 4 we outline the exploitation of the method presented in Section 2 for the assembly of the mass and stiffness matrices appearing in the DG formulation. Several two– and three–dimensional numerical results are presented in Section 5 in order to show the efficiency of the proposed approach.

2 Integrating polynomials over general polygons/polyhedra

In this section we review the procedure introduced by Chin, Lasserre, and Sukumar in [26] for the integration of homogeneous functions over a polytopic domain. To this end, we consider the numerical computation of $\int_{\mathscr{P}} g(\mathbf{x})\mathrm{d}\mathbf{x}$, where

- $\mathscr{P} \subset \mathbb{R}^d$, $d = 2, 3$, is a closed polytope, whose boundary $\partial\mathscr{P}$ is defined by m $(d-1)$–dimensional *faces* $\mathcal{F}_i$, $i = 1, \ldots, m$. Each *face* $\mathcal{F}_i$ lies in a hyperplane $\mathcal{H}_i$ identified by a vector $\mathbf{a}_i \in \mathbb{R}^d$ and a scalar number b_i, such that

$$\mathbf{x} \in \mathcal{H}_i \iff \mathbf{a}_i \cdot \mathbf{x} = b_i, \quad i = 1, \ldots, m. \tag{1}$$

  We observe that $\mathbf{a}_i$, $i = 1, \ldots, m$, can be chosen as the unit outward normal vector to $\mathcal{F}_i$, $i = 1, \ldots, m$, respectively, relative to $\mathscr{P}$, cf. Figures 1 and 2.

- $g : \mathscr{P} \to \mathbb{R}$ is a *homogeneous function* of degree $q \in \mathbb{R}$, i.e.,

$$\forall \lambda > 0, \quad g(\lambda\mathbf{x}) = \lambda^q g(\mathbf{x}) \quad \forall \mathbf{x} \in \mathscr{P}.$$

We recall that Euler's homogeneous function theorem [55] states that, if g is a *homogeneous function* of degree $q \geq 0$, then the following identity holds:

$$q\ g(\mathbf{x}) = \nabla g(\mathbf{x}) \cdot \mathbf{x} \quad \forall \mathbf{x} \in \mathbb{R}^d. \tag{2}$$

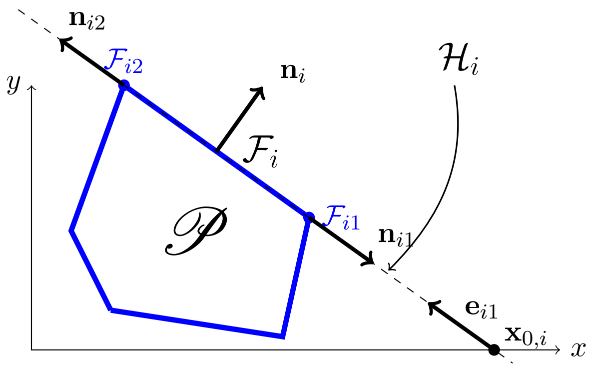

Figure 1: Example of a two–dimensional polytope $\mathscr{P}$ and its face $\mathcal{F}_i$. The variety $\mathcal{H}_i$ is defined by the local origin $\mathbf{x}_{0,i}$ and the vector $\mathbf{e}_{i1}$.

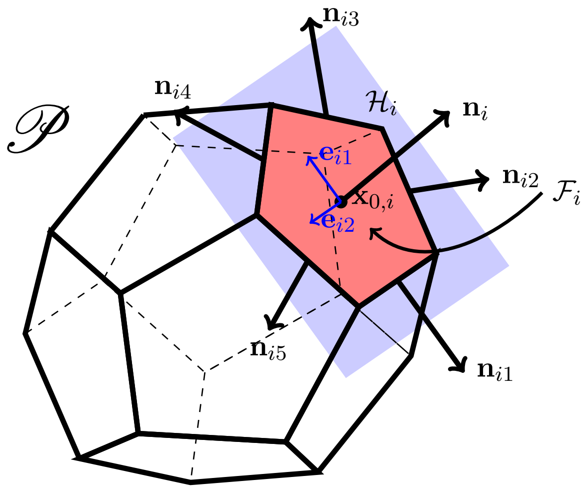

Figure 2: The dodecahedron $\mathscr{P}$ with pentagonal faces and the face $\mathcal{F}_i \subset \partial\mathscr{P}$ with unit outward normal vector $\mathbf{n}_i$. Here, $\mathcal{F}_i$ has five edges $\mathcal{F}_{ij}, j = 1, \dots, 5$ and five unit outward normal vectors $\mathbf{n}_{ij}$, $j = 1, \dots, 5$, lying on the plane $\mathcal{H}_i$. The variety $\mathcal{H}_i$ is identified by the local origin $\mathbf{x}_{0,i}$ and the orthonormal vectors $\mathbf{e}_{i1}, \mathbf{e}_{i2}$.

Next we introduce the generalized Stokes' theorem, which can be stated as follows (see [63] for details): given a generic vector field $\mathbf{X} : \mathscr{P} \to \mathbb{R}^d$, the following identity holds

$$\int_{\mathscr{P}} (\nabla \cdot \mathbf{X}(\mathbf{x}))g(\mathbf{x})\mathrm{d}\mathbf{x} + \int_{\mathscr{P}} \nabla g(\mathbf{x}) \cdot \mathbf{X}(\mathbf{x})\mathrm{d}\mathbf{x} = \int_{\partial\mathscr{P}} \mathbf{X}(\mathbf{x}) \cdot \mathbf{n}(\mathbf{x})g(\mathbf{x})\mathrm{d}\sigma, \tag{3}$$

where $\mathbf{n}$ is the unit outward normal vector to $\mathscr{P}$. Selecting $\mathbf{X} = \mathbf{x}$ in (3), and employing (2), we deduce that

$$\int_{\mathscr{P}} g(\mathbf{x})\mathrm{d}\mathbf{x} = \frac{1}{d+q}\int_{\partial\mathscr{P}} \mathbf{x} \cdot \mathbf{n}(\mathbf{x})g(\mathbf{x})\mathrm{d}\sigma = \frac{1}{d+q}\sum_{i=1}^{m} b_i \int_{\mathcal{F}_i} g(\mathbf{x})\ \mathrm{d}\sigma. \tag{4}$$

Equation (4) states that if g is *homogeneous*, then the integral of g over a polytope $\mathscr{P}$ can be evaluated by computing the integral of the same function over the boundary faces $\mathcal{F}_i \subset \partial\mathscr{P}$, $i = 1, \dots, m$. By applying Stokes' theorem recursively, we can further reduce each term $\int_{\mathcal{F}_i} g(\mathbf{x})\mathrm{d}\sigma$, $i = 1, \dots, m$, to the integration over $\partial\mathcal{F}_i$, $i = 1, \dots, m$, respectively. To this end, Stokes' theorem needs to be applied on the hyperplane $\mathcal{H}_i$, $i = 1, \dots, m$, in which each $\mathcal{F}_i,\ i=1,\dots,m$, lies, respectively. In order to proceed, let $\boldsymbol{\gamma}:\mathbb{R}^{d-1}\to\mathbb{R}^d$ be the function which expresses a generic point $\tilde{\mathbf{x}}=(\tilde{x}_1,\dots,\tilde{x}_{d-1})^\top\in\mathbb{R}^{d-1}$ as a point in $\mathbb{R}^d$ that lies on $\mathcal{H}_i,\ i=1,\dots,m$, i.e.,

$$\tilde{\mathbf{x}}\longmapsto\boldsymbol{\gamma}(\tilde{\mathbf{x}})=\mathbf{x}_{0,i}+\sum_{n=1}^{d-1}\tilde{x}_n\mathbf{e}_{in},\quad\text{with}\ \ \mathbf{e}_{in}\in\mathbb{R}^d,\ \ \mathbf{e}_{in}\cdot\mathbf{e}_{im}=\delta_{nm}.$$

Here, $\mathbf{x}_{0,i}\in\mathcal{H}_i,\ i=1,\dots,m$, is an arbitrary point which represents the origin of the coordinate system on $\mathcal{H}_i$, and $\{\mathbf{e}_{in}\}_{n=1}^{d-1}$ is an orthonormal basis on $\mathcal{H}_i,\ i=1,\dots,m$; see Figures 1 and 2 for two– and three–dimensional examples, respectively. Notice that $\mathbf{x}_{0,i}$ does not have to lie inside $\mathcal{F}_i,\ i=1,\dots,m$. Let $\widetilde{\mathcal{F}_i}\subset\mathbb{R}^{d-1}$ such that $\boldsymbol{\gamma}(\widetilde{\mathcal{F}_i})=\mathcal{F}_i,\ i=1,\dots,m$, then the following identity holds:

$$\int_{\mathcal{F}_i}g(\mathbf{x})\mathrm{d}\sigma=\int_{\widetilde{\mathcal{F}_i}}g(\boldsymbol{\gamma}(\tilde{\mathbf{x}}))\mathrm{d}\tilde{\mathbf{x}},\quad i=1,\dots,m.\tag{5}$$

Before outlining the details regarding the recursive application of the Stokes' Theorem to (4), we need to show the following lemma.

Lemma 2.1. *Let $\mathcal{F}_{ij}\subset\partial\mathcal{F}_i$ $j=1,\dots,m_i$, be the vertices/edges of $\mathcal{F}_i,\ i=1,\dots,m$, for $d=2,3$, respectively, and let $\mathbf{n}_{ij}$ be the unit outward normal vectors to $\mathcal{F}_{ij}$ lying in $\mathcal{H}_i$. Moreover, let $\widetilde{\mathcal{F}_{ij}}\subset\partial\widetilde{\mathcal{F}_i}$ be the preimage of $\mathcal{F}_{ij}$ with respect to the map $\boldsymbol{\gamma}$, and $\tilde{\mathbf{n}}_{ij}$ be the corresponding unit outward normal vector. Then, the following identity holds*

$$\tilde{\mathbf{n}}_{ij}=\underline{\mathbf{E}}^\top\mathbf{n}_{ij},\quad i=1,\dots,m,\ j=1,\dots,m_i,\tag{6}$$

where $\underline{\mathbf{E}}\in\mathbb{R}^{d\times(d-1)}$, whose columns are the vectors $\{\mathbf{e}_{in}\}_{n=1}^{d-1},\ i=1,\dots,m$.

Proof. Before we begin, we first note that employing the definition of $\boldsymbol{\gamma}$ we have that

$$\mathbf{x}=\boldsymbol{\gamma}(\tilde{\mathbf{x}})=\mathbf{x}_{0,i}+\underline{\mathbf{E}}\tilde{\mathbf{x}},\qquad\text{i.e.,}\qquad\mathbf{x}-\mathbf{x}_{0,i}=\underline{\mathbf{E}}\tilde{\mathbf{x}}.\tag{7}$$

We distinguish between the two cases $d=2$ and $d=3$. If $d=2$, then $\mathcal{F}_{ij},\ j=1,2$, are the two vertices of the edge $\mathcal{F}_i,\ i=1,\dots,m$. In this case the vectors $\mathbf{n}_{ij}$ and $\tilde{\mathbf{n}}_{ij}$ can be defined as

$$\tilde{\mathbf{n}}_{i1}=\frac{\widetilde{\mathcal{F}_{i1}}-\widetilde{\mathcal{F}_{i2}}}{\|\widetilde{\mathcal{F}_{i1}}-\widetilde{\mathcal{F}_{i2}}\|},\quad\mathbf{n}_{i1}=\frac{\mathcal{F}_{i1}-\mathcal{F}_{i2}}{\|\mathcal{F}_{i1}-\mathcal{F}_{i2}\|},\quad\tilde{\mathbf{n}}_{i2}=-\tilde{\mathbf{n}}_{i1},\quad\mathbf{n}_{i2}=-\mathbf{n}_{i1}.$$

Thereby, exploiting (7) and the identity $\underline{\mathbf{E}}^\top\underline{\mathbf{E}}=\underline{\mathbf{I}}$, where $\underline{\mathbf{I}}$ denotes the identity matrix, we observe that

$$\widetilde{\mathcal{F}_{i1}}-\widetilde{\mathcal{F}_{i2}}=\underline{\mathbf{E}}^\top(\mathcal{F}_{i1}-\mathbf{x}_{0,i})-\underline{\mathbf{E}}^\top(\mathcal{F}_{i2}-\mathbf{x}_{0,i})=\underline{\mathbf{E}}^\top(\mathcal{F}_{i1}-\mathcal{F}_{i2});$$

hence

$$\|\widetilde{\mathcal{F}_{i1}}-\widetilde{\mathcal{F}_{i2}}\|=\sqrt{(\mathcal{F}_{i1}-\mathcal{F}_{i2})^\top\underline{\mathbf{E}}\underline{\mathbf{E}}^\top(\mathcal{F}_{i1}-\mathcal{F}_{i2})}=\|\mathcal{F}_{i1}-\mathcal{F}_{i2}\|,$$

from which (6) follows immediately. If $d=3$, then for a given pair $i,j,\ i=1,\dots,m$, $j=1,\dots,m_i$, let $\tilde{\mathbf{x}}_a,\tilde{\mathbf{x}}_b\in\mathbb{R}^{d-1}$ be such that $\tilde{\mathbf{n}}_{ij}=\tilde{\mathbf{x}}_b-\tilde{\mathbf{x}}_a$, and let $\tilde{\mathbf{x}}_1,\tilde{\mathbf{x}}_2$ be the vertices of $\widetilde{\mathcal{F}_{ij}}$. Then, we note that

$$\|\tilde{\mathbf{x}}_b-\tilde{\mathbf{x}}_a\|=\|\tilde{\mathbf{n}}_{ij}\|=1,\quad(\tilde{\mathbf{x}}_b-\tilde{\mathbf{x}}_a)\cdot(\tilde{\mathbf{x}}_2-\tilde{\mathbf{x}}_1)=0.\tag{8}$$

Moreover, from the relation $\mathbf{x}_\diamond = \mathbf{x}_{0,i} + \underline{\mathbf{E}}\tilde{\mathbf{x}}_\diamond$, where $\diamond \in \{a, b, 1, 2\}$, we have that

$$\tilde{\mathbf{n}}_{ij} = \underline{\mathbf{E}}^\top(\mathbf{x}_b - \mathbf{x}_a), \quad (\mathbf{x}_b - \mathbf{x}_a) = \underline{\mathbf{E}}\tilde{\mathbf{n}}_{ij}.$$

To complete the proof we must show that $(\mathbf{x}_b - \mathbf{x}_a) = \mathbf{n}_{ij}$. To this end, we need to prove that $(\mathbf{x}_b - \mathbf{x}_a)$ has unitary norm and that it is normal to the face. Using the previous relation together with (8), we have

$$\|\mathbf{x}_b - \mathbf{x}_a\| = \|\underline{\mathbf{E}}\tilde{\mathbf{n}}_j\| = \sqrt{\tilde{\mathbf{n}}_j^\top \underline{\mathbf{E}}^\top \underline{\mathbf{E}}\tilde{\mathbf{n}}_j} = \sqrt{\tilde{\mathbf{n}}_j^\top \ \underline{\mathbf{I}} \ \tilde{\mathbf{n}}_j} = 1,$$

and

$$(\mathbf{x}_b - \mathbf{x}_a) \cdot (\mathbf{x}_2 - \mathbf{x}_1) = (\tilde{\mathbf{x}}_b - \tilde{\mathbf{x}}_a)\underline{\mathbf{E}}^\top \underline{\mathbf{E}}(\mathbf{x}_2 - \mathbf{x}_1) = 0,$$

from which (6) follows. □

Given identity (5) and Lemma 2.1, we can prove the following result.

Proposition 2.2. *Let $\mathcal{F}_i$, $i = 1, \dots, m$, be a face of the polytope $\mathscr{P}$, and let $\mathcal{F}_{ij}$, $j = 1, \dots, m_i$ be the planar/straight faces/edges such that $\partial\mathcal{F}_i = \cup_{j=1}^{m_i}\mathcal{F}_{ij}$ for some $m_i \in \mathbb{N}$. Then, for any homogeneous function g, of degree $q \geq 0$, the following identity holds*

$$\int_{\mathcal{F}_i} g(\mathbf{x})\mathrm{d}\sigma = \frac{1}{d-1+q}\Big(\sum_{j=1}^{m_i} d_{ij} \int_{\mathcal{F}_{ij}} g(\mathbf{x})\mathrm{d}\nu \ + \ \int_{\mathcal{F}_i} \mathbf{x}_{0,i} \cdot \nabla g(\mathbf{x})\mathrm{d}\sigma\Big),$$

where d_{ij} denotes the algebraic distance between $\mathcal{F}_{ij}$ and $\mathbf{x}_{0,i}$, $i = 1, \dots, m$, and $\mathbf{x}_{0,i} \in \mathcal{H}_i$, $i = 1, \dots, m$, is arbitrary.

Proof. If we denote by $\nabla_i = \left[\frac{\partial}{\partial\tilde{x}_1}, \dots, \frac{\partial}{\partial\tilde{x}_{d-1}}\right]^\top$ the gradient operator on the variety $\mathcal{H}_i$, $i = 1, \dots, m$, with respect to the coordinate system $(\tilde{x}_1, \dots, \tilde{x}_{d-1})$, then, upon application of Stokes' theorem, we have

$$\underbrace{\int_{\widetilde{\mathcal{F}}_i} (\nabla_i \cdot \widetilde{\mathbf{X}}) g(\boldsymbol{\gamma}(\tilde{\mathbf{x}}))\mathrm{d}\tilde{\mathbf{x}}}_{①} \ + \ \underbrace{\int_{\widetilde{\mathcal{F}}_i} \widetilde{\mathbf{X}} \cdot \nabla_i g(\boldsymbol{\gamma}(\tilde{\mathbf{x}}))\mathrm{d}\tilde{\mathbf{x}}}_{②} = \underbrace{\int_{\partial\widetilde{\mathcal{F}}_i} \widetilde{\mathbf{X}} \cdot \tilde{\mathbf{n}} \ g(\boldsymbol{\gamma}(\tilde{\mathbf{x}}))\mathrm{d}\nu(\tilde{\mathbf{x}})}_{③}, \tag{9}$$

where $\tilde{\mathbf{n}}$ is the unit outward normal vector of $\widetilde{\mathcal{F}}_i$ and $\widetilde{\mathbf{X}}$ is a vector field on $\mathbb{R}^{d-1}$. Next, we transform (9) back to the original coordinate system. To this end, denoting $\underline{\mathbf{E}} \in \mathbb{R}^{d\times(d-1)}$ to be the matrix whose columns are the vectors $\{\mathbf{e}_{in}\}_{n=1}^{d-1}$, we observe that, if we choose $\widetilde{\mathbf{X}} = \tilde{\mathbf{x}}$, then its divergence is $\nabla_i \cdot \widetilde{\mathbf{X}} = d - 1$. Exploiting (7), the term $\nabla_i g(\boldsymbol{\gamma}(\tilde{\mathbf{x}}))$ can be written as follows:

$$\nabla_i g(\boldsymbol{\gamma}(\tilde{\mathbf{x}})) = \begin{bmatrix} \frac{\partial\gamma_1}{\partial\tilde{x}_1} & \frac{\partial\gamma_2}{\partial\tilde{x}_1} & \cdots & \frac{\partial\gamma_d}{\partial\tilde{x}_1} \\ \frac{\partial\gamma_1}{\partial\tilde{x}_2} & \frac{\partial\gamma_2}{\partial\tilde{x}_2} & \cdots & \frac{\partial\gamma_d}{\partial\tilde{x}_2} \\ \vdots & \vdots & \ddots & \vdots \\ \frac{\partial\gamma_1}{\partial\tilde{x}_{d-1}} & \frac{\partial\gamma_2}{\partial\tilde{x}_{d-1}} & \cdots & \frac{\partial\gamma_d}{\partial\tilde{x}_{d-1}} \end{bmatrix} \begin{bmatrix} \frac{\partial g}{\partial\tilde{x}_1} \\ \frac{\partial g}{\partial\tilde{x}_2} \\ \vdots \\ \frac{\partial g}{\partial\tilde{x}_d} \end{bmatrix} = (\underline{\mathbf{E}}^\top \nabla g)(\boldsymbol{\gamma}(\tilde{\mathbf{x}})). \tag{10}$$

Exploiting (7) and (10), we can write ① and ② as

$$① = (d-1)\int_{\widetilde{\mathcal{F}}_i} g(\boldsymbol{\gamma}(\tilde{\mathbf{x}}))\mathrm{d}\tilde{\mathbf{x}} = (d-1)\int_{\mathcal{F}_i} g(\mathbf{x})\mathrm{d}\sigma, \tag{11}$$

$$②= \int_{\widetilde{\mathcal{F}}_i} \tilde{\mathbf{x}}^\top \underline{\mathbf{E}}^\top \nabla g(\boldsymbol{\gamma}(\tilde{\mathbf{x}}))\mathrm{d}\tilde{\mathbf{x}} = \int_{\mathcal{F}_i} (\mathbf{x}-\mathbf{x}_{0,i})\cdot \nabla g(\mathbf{x})\mathrm{d}\sigma \tag{12}$$
$$= q \int_{\mathcal{F}_i} g(\mathbf{x})\mathrm{d}\sigma \;-\; \int_{\mathcal{F}_i} \mathbf{x}_{0,i}\cdot \nabla g(\mathbf{x})\mathrm{d}\sigma,$$

respectively. Employing Lemma 2.1, together with (7), we have that

$$③ = \sum_{j=1}^{m_i} \int_{\widetilde{\mathcal{F}_{ij}}} \tilde{\mathbf{x}}^\top \tilde{\mathbf{n}}_{ij} g(\boldsymbol{\gamma}(\tilde{\mathbf{x}}))\mathrm{d}\nu(\tilde{\mathbf{x}}) \tag{13}$$
$$= \sum_{j=1}^{m_i} \int_{\mathcal{F}_{ij}} (\mathbf{x}-\mathbf{x}_{0,i})^\top \underline{\mathbf{E}}\underline{\mathbf{E}}^\top \mathbf{n}_{ij} g(\mathbf{x})\mathrm{d}\nu(\mathbf{x}) = \sum_{j=1}^{m_i} \int_{\mathcal{F}_{ij}} (\mathbf{x}-\mathbf{x}_{0,i})\cdot \mathbf{n}_{ij} g(\mathbf{x})\mathrm{d}\nu.$$

We observe that the term $(\mathbf{x}-\mathbf{x}_{0,i})\cdot\mathbf{n}_{ij}$ is constant for any $\mathbf{x}\in\mathcal{F}_{ij}$, and that it represents the algebraic distance between $\mathcal{F}_{ij}$ and $\mathbf{x}_{0,i}$; thereby, we define $d_{ij} = (\mathbf{x}-\mathbf{x}_{0,i})\cdot\mathbf{n}_{ij}$. From the above identities (11), (12) and (13) we deduce the statement of the Proposition. □

Using Proposition 2.2, together with equation (4), we obtain the following identity

$$\int_{\mathscr{P}} g(\mathbf{x})\mathrm{d}\mathbf{x} = \frac{1}{d+q}\sum_{i=1}^{m} \frac{b_i}{d-1+q}\Big(\sum_{j=1}^{m_i} d_{ij}\int_{\mathcal{F}_{ij}} g(\mathbf{x})\mathrm{d}\nu \;+\; \int_{\mathcal{F}_i} \mathbf{x}_{0,i}\cdot\nabla g(\mathbf{x})\mathrm{d}\sigma\Big), \tag{14}$$

where we recall that $\partial\mathscr{P} = \cup_{i=1}^{m}\mathcal{F}_i$ and $\partial\mathcal{F}_i = \cup_{j=1}^{m_i}\mathcal{F}_{ij}$, for $i=1,\ldots,m$.

Remark 1. If $d=2$, then $\mathcal{F}_{ij}$ is a point and (14) states that the integral of g on $\mathscr{P}$ con be computed by vertex-evaluations of the integrand plus a line integration of the partial derivative of g. If $d=3$ we can apply Stokes' Theorem recursively to $\int_{\mathcal{F}_{ij}} g(\mathbf{x})\mathrm{d}\nu$. Proceeding as before, we get

$$\int_{\mathcal{F}_{ij}} g(\mathbf{x})\mathrm{d}\nu = \frac{1}{d-2+q}\Big(\sum_{k=1}^{m_{ij}} d_{ijk}\int_{\mathcal{F}_{ijk}} g(\mathbf{x})\mathrm{d}\xi \;+\; \int_{\mathcal{F}_{ij}} \mathbf{x}_{0,ij}\cdot\nabla g(\mathbf{x})\mathrm{d}\nu\Big),$$

where $\partial\mathcal{F}_{ij} = \cup_{k=1}^{m_{ij}}\mathcal{F}_{ijk}$, $\mathbf{x}_{0,ij}\in\mathcal{F}_{ij}$ is arbitrarly chosen, and d_{ijk} is the algebraic distance between $\mathcal{F}_{ijk}$ and $\mathbf{x}_{0,ij}$.

In view of the application of Proposition 2.2 to finite element methods, we are interested in the integration of a particular class of *homogeneous functions*, namely *polynomial homogeneous functions* of the form

$$g(\mathbf{x}) = x_1^{k_1}x_2^{k_2}\cdots x_d^{k_d}, \quad \text{where } k_n\in\mathbb{N}_0 \text{ for } n=1,\ldots,d.$$

In this case, g is a *homogeneous function* of degree $q = k_1+\cdots+k_d$, and the general partial derivative $\frac{\partial g}{\partial x_n}$ is a *homogeneous function* of degree $q-1 = k_1+\cdots+k_d-1$. With this in mind, it is possible to recursively apply formula (14) to the terms involving the integration of the derivatives of g. To this end, we write $\mathcal{E}\subset\mathbb{R}^d$, $d=2,3$, be a N-polytopic domain of integration, with $N=1,\ldots,d$, and let $\partial\mathcal{E} = \cup_{i=1}^{m}\mathcal{E}_i$, where each $\mathcal{E}_i\subset\mathbb{R}^d$ is a $(N-1)$-polytopic domain. For $d=2,3$, $\mathcal{E}_i,\ i=1,\ldots,m$, will be an edge or a polygonal face, respectively; see Table 1 for details. We define the function

$$\mathcal{I}(N,\mathcal{E},k_1,\ldots,k_d) = \int_{\mathcal{E}} x_1^{k_1}\ldots x_d^{k_d}\;\mathrm{d}\sigma_N(x_1,\ldots,x_d), \tag{15}$$

that returns the integral of the polynomial $x_1^{k_1}\ldots x_d^{k_d}$ over $\mathcal{E}$, where $\mathrm{d}\sigma_N$ is the N–dimensional differential operator, $N=1,2,\ldots,d$. According to Proposition 2.2, the recursive definition of the function $\mathcal{I}$ is given in Algorithm 1.

Algorithm 1 $\mathcal{I}(N,\mathcal{E},k_1,\ldots,k_d) = \int_{\mathcal{E}} x_1^{k_1}\ldots x_d^{k_d}\ \mathrm{d}\sigma_N(x_1,\ldots,x_d)$

if $N=0$ ($\mathcal{E}=(v_1,\ldots,v_d)\in\mathbb{R}^d$ is a point)

$$\textbf{return}\quad \mathcal{I}(N,\mathcal{E},k_1,\ldots,k_d) = v_1^{k_1}\cdots v_d^{k_d};$$

else if $1\le N\le d-1$ ($\mathcal{E}$ is a point if $d=1$ or an edge if $d=2$ or a face if $d=3$)

$$\begin{aligned}\mathcal{I}(N,\mathcal{E},k_1,\ldots,k_d) = \frac{1}{N+\sum_{n=1}^{d}k_n}\Big(&\sum_{i=1}^{m} d_i\ \mathcal{I}(N-1,\mathcal{E}_i,k_1,\ldots,k_d)\\ &+x_{0i,1}\ k_1\ \mathcal{I}(N,\mathcal{E},k_1-1,k_2,\ldots,k_d)\\ &+\cdots+\ x_{0i,d}\ k_d\ \mathcal{I}(N,\mathcal{E},k_1,\ldots,k_d-1)\Big);\end{aligned}$$

else if $N=d$ ($\mathcal{E}$ is an interval if $d=1$ or a polygon if $d=2$ or a polyhedron if $d=3$)

$$\mathcal{I}(N,\mathcal{E},k_1,\ldots,k_d) = \frac{1}{N+\sum_{n=1}^{d}k_n}\Big(\sum_{i=1}^{m} b_i\ \mathcal{I}(N-1,\mathcal{E}_i,k_1,\ldots,k_d)\Big).$$

end if

Table 1 Polytopic domains of integration $\mathcal{E}$ considered in Algorithm 1 as a function of the dimension d.

	$N=3$	$N=2$	$N=1$	$N=0$
$d=3$	$\mathcal{E}=\mathscr{P}$ is a polyhedron	$\mathcal{E}=\mathcal{F}_i\subset\partial\mathscr{P}$ is a polygon	$\mathcal{E}=\mathcal{F}_{ij}\subset\partial\mathcal{F}_i$ is an edge	$\mathcal{E}=\mathcal{F}_{ijk}\subset\partial\mathcal{F}_{ij}$ is a point
$d=2$		$\mathcal{E}=\mathscr{P}$ is a polygon	$\mathcal{E}=\mathcal{F}_i\subset\partial\mathscr{P}$ is an edge	$\mathcal{E}=\mathcal{F}_{ij}\subset\partial\mathcal{F}_i$ is a point
$d=1$			$\mathcal{E}=\mathscr{P}$ is an interval	$\mathcal{E}=\mathcal{F}_i\subset\partial\mathscr{P}$ is a point

Remark 2. When $1\le N\le d-1$ the point $\mathbf{x}_{0,i}=(x_{0i,1},\ldots,x_{0i,d})\in\mathcal{E}$ is arbitrarily chosen and represents the origin of the coordinate system on $\mathcal{H}_i$, whereas d_i represents the algebraic distance between $\mathcal{E}_i$ and $\mathbf{x}_{0,i},\ i=1,\ldots,m$.
Remark 3. We remark that in Algorithm 1, $b_i,\ i=1,\ldots,m$, is the same constant appearing in (1). Here it can be evaluated as $b_i=\mathbf{n}_i\cdot\mathbf{v}$, where $\mathbf{v}$ is a vertex of $\mathcal{E}_i$ and $\mathbf{n}_i$ is the unit outward normal vector, $i=1,\ldots,m$.
Remark 4. We point out that in formula (14), as well as in (15), the shape of the underlying polytope can be general; for example convex/non convex simply-connected domains $\mathcal{E}$ are allowed.

2.1 Integration of bivariate polynomials over polygonal domains

In order to test the performance of the method proposed in Algorithm 1, we consider the integration of bivariate *homogeneous functions* on a given polygon $\mathscr{P}\subset\mathbb{R}^2$ based on using the three different approaches:

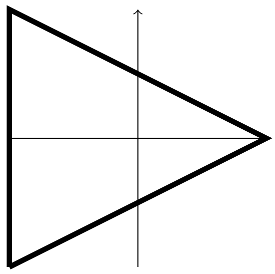

Figure 3: Triangle ($\mathscr{P}_1$).

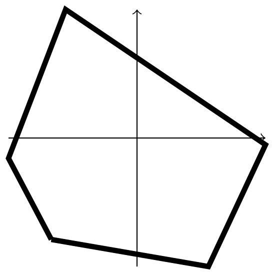

Figure 4: Irregular polygon with 5 faces ($\mathscr{P}_2$).

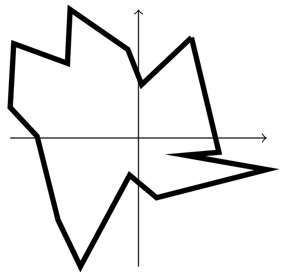

Figure 5: Irregular polygon with 15 faces ($\mathscr{P}_3$).

Table 2 Coordinates of the polygons of Figures 3, 4, and 5.

	vertex	x-cordinates	y-cordinates
	1	−1.000000000000000	−1.000000000000000
$\mathscr{P}_1$	2	1.000000000000000	0.000000000000000
	3	−1.000000000000000	1.000000000000000
	1	−0.666666666666667	−0.789473684210526
	2	0.555555555555556	−1.000000000000000
$\mathscr{P}_2$	3	1.000000000000000	−0.052631578947368
	4	−0.555555555555556	1.000000000000000
	5	−1.000000000000000	−0.157894736842105
	1	0.413048522141662	0.781696234443715
	2	0.024879797655533	0.415324992429711
	3	−0.082799691823524	0.688810136531751
	4	−0.533191422779328	1.000000000000000
	5	−0.553573605852999	0.580958514816226
	6	−0.972432940212767	0.734117068746903
	7	−1.000000000000000	0.238078507228890
$\mathscr{P}_3$	8	−0.789986179147920	0.012425068086110
	9	−0.627452906935866	−0.636532897516109
	10	−0.452662174765764	−1.000000000000000
	11	−0.069106265580153	−0.289054989277619
	12	0.141448047807069	−0.464417038155806
	13	1.000000000000000	−0.245698820584615
	14	0.363704451489016	−0.134079689960635
	15	0.627086024018283	−0.110940423607648

A.1 Recursive algorithm described in Section 2, based on the formula (15):

$$\int_{\mathscr{P}} x^k\, y^l \mathrm{d}\mathbf{x} = \mathcal{I}(2, \mathscr{P}, k, l),$$

cf. also Algorithm 1.

A.2 Use of the formula (4) together with numerical integration employed for the evaluation of the face integrals with known one–dimensional Gaussian quadrature rule as recently proposed in [27];

A.3 Exploiting sub-tessellation technique: the domain of integration $\mathscr{P}$ is firstly decomposed into triangles where classical Gaussian quadrature rules are then employed.

We test the three different approaches for integrating bivariate polynomials of different polynomial degrees on the triangle depicted in Figure 3 and the two irregular polygons shown in Figures 4 and 5, cf. Table 2 for the list of coordinates for each domain; the actual values of the integrals are given in Table 3. In Table 4 we show the average CPU-time

Table 3 The approximated values of the integral over the three polygons in Figures 3, 4 and 5 obtained with approach **A.1**.

	$\mathcal{E} = \mathscr{P}_1$	$\mathcal{E} = \mathscr{P}_2$	$\mathcal{E} = \mathscr{P}_3$
$\int_{\mathcal{E}} x^5y^5$	0	-0.0020324991	-0.002589861
$\int_{\mathcal{E}} x^{10}y^{10}$	0.0111339078	$7.4274779926 \times 10^{-5}$	$1.5738050178 \times 10^{-4}$
$\int_{\mathcal{E}} x^{20}y^{20}$	0.0030396808	$6.0738145408 \times 10^{-8}$	$1.3793481020 \times 10^{-6}$
$\int_{\mathcal{E}} x^{40}y^{40}$	$7.9534562047 \times 10^{-4}$	$2.2238524572 \times 10^{-12}$	$4.2588831784 \times 10^{-10}$
$\int_{\mathcal{E}} x^{10}y^5$	0	$-2.0911953867 \times 10^{-4}$	0.0014996521
$\int_{\mathcal{E}} x^{20}y^5$	0	$-1.3797380205 \times 10^{-5}$	$7.0356275077 \times 10^{-4}$
$\int_{\mathcal{E}} x^{40}y^5$	0	$-7.9203571311 \times 10^{-7}$	$2.5065856538 \times 10^{-4}$
$\int_{\mathcal{E}} x^5y^{20}$	-0.005890191	$8.08469022058 \times 10^{-5}$	$-1.330384913 \times 10^{-4}$
$\int_{\mathcal{E}} x^5y^{40}$	-0.001868889	$4.37593748009 \times 10^{-5}$	$-3.963064075 \times 10^{-5}$

Table 4 CPU times as a function of the integrand and the integration domain $\mathscr{P}$ for the three approaches **A.1**, **A.2** and **A.3**.

	$\mathscr{P}_1$			$\mathscr{P}_2$			$\mathscr{P}_3$		
	A.1	**A.2**	**A.3**	**A.1**	**A.2**	**A.3**	**A.1**	**A.2**	**A.3**
x^5y^5	0.054	0.159	0.616	0.083	0.244	0.973	0.227	0.678	2.856
$x^{10}y^{10}$	0.078	0.221	1.359	0.123	0.328	2.321	0.351	0.939	7.301
$x^{20}y^{20}$	0.124	0.344	4.060	0.207	0.540	7.399	0.580	1.498	22.70
$x^{40}y^{40}$	0.208	0.578	14.79	0.377	0.934	27.24	1.073	2.671	86.63
$x^{10}y^5$	0.064	0.191	0.999	0.081	0.296	1.699	0.237	0.833	5.125
$x^{20}y^5$	0.078	0.240	1.955	0.089	0.412	3.690	0.274	1.093	10.99
$x^{40}y^5$	0.107	0.363	4.975	0.085	0.616	9.504	0.332	1.680	29.40
x^5y^{20}	0.052	0.244	1.971	0.085	0.412	3.662	0.243	1.117	11.07
x^5y^{40}	0.051	0.365	5.009	0.082	0.597	9.295	0.272	1.673	29.17

taken to evaluate the underlying integral using each method. We point out that, for each integrand and each integration domain $\mathscr{P}$, the relative errors between the output of the three different approaches are of the order of machine precision; that is, all three algorithms return the exact integral up to roundoff error. The results shown in Table 4 illustrate that the sub-tessellation approach **A.3** is the slowest while the proposed method **A.1** is the fastest for all of the considered cases; in particular, we highlight that, even for just a single domain of integration, the former method is between one- to two-orders of magnitude slower than the latter approach proposed in this article. Moreover, when the integration domain consists of a triangle, our algorithm **A.1** still outperforms classical quadrature rules, cf. Algorithm **A.3**, even though in this case no subtessellation is undertaken. When comparing **A.1** and **A.2**, we observe that the former algorithm is again superior in terms of CPU time in comparison with the latter approach; this difference seems to grow when the exponents k and l of the integrand function x^ky^l are very different. This is because in **A.1** we made an optimal choice of the point $\mathbf{x}_{0,i} = (x_{0i,1}, x_{0i,2})^\top$ appearing in (14). Indeed, performing the geometric reduction of the face of the domain of integration, we then choose $x_{0i,1} = 0$ or $x_{0i,2} = 0$ if the exponents of the integrand function x^ky^l are $k \geq l$ or $k < l$, respectively. The choice $x_{0i,1} = 0$ or $x_{0i,2} = 0$ allows us to avoid the recursive calls to the function $\mathcal{I}$ related to the x– or y–partial derivatives, respectively. In this way the approach **A.1** is able to exploit the form of the integrand in order to optimize the evaluation of the corresponding integral.

3 Application to hp-version DG methods

We consider the following weak formulation of the diffusion-reaction model problem, subject to a homogeneous Dirichlet boundary condition, given by: find $u \in V = H_0^1(\Omega)$ such that

$$\int_\Omega \nabla u \cdot \nabla v \, \mathrm{d}x \; + \int_\Omega uv \mathrm{d}x = \int_\Omega fv \, \mathrm{d}x \qquad \forall v \in V, \tag{16}$$

with $\Omega \subset \mathbb{R}^d$, $d = 2, 3$, a polygonal/polyhedral domain with Lipschitz boundary and f a given function in $L^2(\Omega)$.

In order to discretize problem (16), we introduce a partition $\mathcal{T}_h$ of the domain Ω, which consists of disjoint (possibly non-convex) open polygonal/polyhedral elements κ of diameter h_κ, such that $\overline{\Omega} = \bigcup_{\kappa\in\mathcal{T}_h} \bar{\kappa}$. We denote the mesh size of $\mathcal{T}_h$ by $h = \max_{\kappa\in\mathcal{T}_h} h_\kappa$. Furthermore, we define the *faces* of the mesh $\mathcal{T}_h$ as the planar/straight intersections of the $(d-1)$–dimensional facets of neighbouring elements. This implies that, for $d = 2$, a *face* consists of a line segment, while for $d = 3$, the *faces* of $\mathcal{T}_h$ are general shaped polygons; without loss of generality, for the definition of the proceeding DG method we assume that the faces are $(d-1)$-dimensional simplices, cf. [23, 24] for a discussion of this issue. In order to introduce the DG formulation, it is helpful to distinguish between boundary and interior element faces, denoted by $\mathcal{F}_h^B$ and $\mathcal{F}_h^I$, respectively. In particular, we observe that $F \subset \partial\Omega$ for $F \in \mathcal{F}_h^B$, while for any $F \in \mathcal{F}_h^I$ we assume that $F \subset \partial\kappa^\pm$, where $\kappa^\pm$ are two adjacent elements in $\mathcal{T}_h$. Furthermore, we write $\mathcal{F}_h = \mathcal{F}_h^I \cup \mathcal{F}_h^B$ to denote the set of all mesh faces of $\mathcal{T}_h$. For simplicity of presentation we assume that each element $\kappa \in \mathcal{T}_h$ possesses a uniformly bounded number of faces under mesh refinement, cf. [23, 24].

We associate to $\mathcal{T}_h$ the corresponding discontinuous finite element space V_h, defined by $V_h = \{v \in L^2(\Omega) : v|_\kappa \in \mathcal{P}_{p_\kappa}(\kappa), \kappa \in \mathcal{T}_h\}$, where $\mathcal{P}_{p_\kappa}(\kappa)$ denotes the space of polynomials of total degree at most $p_\kappa \geq 1$ on $\kappa \in \mathcal{T}_h$. We refer to [23, 24] for more details.

In order to define the DG method, we introduce the jump and average operators:

$$\begin{aligned}
&[\![\boldsymbol{\tau}]\!] = \boldsymbol{\tau}^+ \cdot \mathbf{n}^+ + \boldsymbol{\tau}^- \cdot \mathbf{n}^-, && \{\!\{\boldsymbol{\tau}\}\!\} = \frac{\boldsymbol{\tau}^+ + \boldsymbol{\tau}^-}{2}, && F \in \mathcal{F}_h^I, \\
&[\![v]\!] = v^+\mathbf{n}^+ + v^-\mathbf{n}^-, && \{\!\{v\}\!\} = \frac{v^+ + v^-}{2}, && F \in \mathcal{F}_h^I, \\
&[\![v]\!] = v^+\mathbf{n}^+, && \{\!\{\boldsymbol{\tau}\}\!\} = \boldsymbol{\tau}^+, && F \in \mathcal{F}_h^B,
\end{aligned} \tag{17}$$

where $v^\pm$ and $\boldsymbol{\tau}^\pm$ denote the traces of sufficiently smooth functions v and $\boldsymbol{\tau}$ on F taken from the interior of $\kappa^\pm$, respectively, and $\mathbf{n}^\pm$ are the unit outward normal vectors to $\partial\kappa^\pm$, respectively, cf. [11].

We then consider the bilinear form $\mathcal{A}_h(\cdot,\cdot) : V_h \times V_h \to \mathbb{R}$, corresponding to the symmetric interior penalty DG method, defined by

$$\begin{aligned}
\mathcal{A}_h(u, v) = &\sum_{\kappa\in\mathcal{T}_h} \int_\kappa \nabla u \cdot \nabla v \; dx - \sum_{F\in\mathcal{F}_h} \int_F \left(\{\!\{\nabla_h u\}\!\} \cdot [\![v]\!] + [\![u]\!] \cdot \{\!\{\nabla_h v\}\!\}\right) \; ds \\
&+ \sum_{F\in\mathcal{F}_h} \int_F \alpha_h [\![u]\!] \cdot [\![v]\!] \; ds,
\end{aligned} \tag{18}$$

where ∇_h denotes the broken gradient operator, defined elementwise, and $\alpha_h \in L^\infty(\mathcal{F}_h)$ denotes the interior penalty stabilization function, whose precise definition, based on the analysis introduced in [23, 24], is given below. To this end, we first need the following definition.

Definition 3.1. Let $\tilde{\mathcal{T}}_h$ be the subset of elements $\kappa \in \mathcal{T}_h$ such that each $\kappa \in \tilde{\mathcal{T}}_h$ can be covered by at most $n_{\mathcal{T}}$ shape-regular simplices $\mathcal{K}_i$, $i = 1, \ldots, n_{\mathcal{T}}$, such that

$$dist(\kappa, \partial\mathcal{K}_i) < C_{as} \frac{diam(\mathcal{K}_i)}{p_\kappa^2}, \text{ and } |\mathcal{K}_i| \geq c_{as}|\kappa|$$

for all $i = 1, \ldots, n_{\mathcal{T}}$, for some $n_{\mathcal{T}} \in \mathbb{N}$, where C_{as} and c_{as} are positive constants, independent of κ and $\mathcal{T}_h$.

Given Definition 3.1, we recall the following inverse inequality; see [23, 24] for a detailed proof.

Lemma 3.1. *Let $\kappa \in \mathcal{T}_h$, $F \subset \partial\kappa$ denote one of its faces, and $\tilde{\mathcal{T}}_h$ be defined as in Definition 3.1. Then, for each $v \in \mathcal{P}_{p_\kappa}(\kappa)$, we have the inverse estimate*

$$\|v\|^2_{L^2(F)} \leq C_{INV}(p_\kappa, \kappa, F)\frac{p_\kappa^2|F|}{|\kappa|}\|v\|^2_{L^2(\kappa)},$$

where

$$C_{INV}(p_\kappa, \kappa, F) := C_{inv}\begin{cases} \min\left\{\frac{|\kappa|}{\sup_{\kappa_\flat^F\subset\kappa}|\kappa_\flat^F|}, p_\kappa^{2(d-1)}\right\}, & \text{if } \kappa \in \tilde{\mathcal{T}}_h, \\ \frac{|\kappa|}{\sup_{\kappa_\flat^F\subset\kappa}|\kappa_\flat^F|}, & \text{if } \kappa \in \mathcal{T}_h \setminus \tilde{\mathcal{T}}_h, \end{cases}$$

and $\kappa_\flat^F$ denotes a d–dimensional simplex contained in κ which shares the face F with $\kappa \in \mathcal{T}_h$. Furthermore, C_{inv} is a positive constant, which if $\kappa \in \tilde{\mathcal{T}}_h$ depends on the shape regularity of the covering of κ given in Definition 3.1, but is always independent of $|\kappa|/\sup_{\kappa_\flat^F\subset\kappa}|\kappa_\flat^F|$, p_κ and v.

Based on Lemma 3.1, together with the analysis presented in [23, 24], the parameter α_h can be defined as follows.

Definition 3.2. Let $\alpha_h : \mathcal{F}_h \to \mathbb{R}_+$ be defined facewise by

$$\alpha_h(x) := C_\alpha \begin{cases} \max\limits_{\kappa\in\{\kappa^+,\kappa^-\}}\left\{C_{INV}(p_\kappa, \kappa, F)\frac{p_\kappa^2|F|}{|\kappa|}\right\}, & x \in F, F \in \mathcal{F}_h^I, F \subset \partial\kappa^\pm, \\ C_{INV}(p_\kappa, \kappa, F)\frac{p_\kappa^2|F|}{|\kappa|}, & x \in F, F \in \mathcal{F}_h^B, F \subset \partial\kappa, \end{cases}$$

with $C_\alpha > C_\alpha^{min}$, where C_α^{min} is a sufficiently large lower bound.

The DG discretization of the problem (16) is given by: find $u_h \in V_h$ such that

$$\mathcal{A}_h(u_h, v_h) + \int_\Omega u_h v_h \,\mathrm{d}x = \int_\Omega f v_h \; dx \quad \forall v_h \in V_h. \tag{19}$$

By fixing a basis $\{\phi_i\}_{i=1}^{N_h}$, N_h denoting the dimension of the discrete space V_h, (19) can be rewritten as: find $\mathbf{U} \in \mathbb{R}^{N_h}$ s.t.

$$(\underline{\mathbf{A}} + \underline{\mathbf{M}})\mathbf{U} = \mathbf{f}, \tag{20}$$

where $\mathbf{f}_i = \int_\Omega f\phi_i \mathrm{d}\mathbf{x}$ $\forall i = 1, \ldots, N_h$, $\underline{\mathbf{A}}$ is the stiffness matrix, given by $\underline{\mathbf{A}}_{ij} = \mathcal{A}_h(\phi_j, \phi_i)$ $\forall i, j = 1, \ldots, N_h$, $\underline{\mathbf{M}}$ is the mass matrix, and $\mathbf{U}$ contains the expansion coefficients of $u_h \in V_h$ with respect to the chosen basis. In order to assemble $(\underline{\mathbf{A}} + \underline{\mathbf{M}})$ we need to compute the following matrices:

$$\mathbf{M}_{i,j} = \int_\Omega \phi_i\phi_j \mathrm{d}\mathbf{x}, \quad \mathbf{V}_{i,j} = \int_\Omega \nabla\phi_i \cdot \nabla\phi_j \; \mathrm{d}\mathbf{x}, \tag{21}$$

$$\mathbf{S}_{i,j} = \sum_{F\in\mathcal{F}_h}\int_F \alpha_h[\![\phi_i]\!] \cdot [\![\phi_j]\!]\mathrm{d}\sigma, \quad \mathbf{I}_{i,j} = \sum_{F\in\mathcal{F}_h}\int_F \{\!\{\nabla\phi_i\}\!\} \cdot [\![\phi_j]\!]\mathrm{d}\sigma, \tag{22}$$

for $i, j = 1, \ldots, N_h$, where as before N_h denotes the dimension of the DG space V_h. In particular, the stiffness matrix related to the DG approximation of problem (19) is defined as

$$\mathbf{A} = \mathbf{V} - \mathbf{I}^\top - \mathbf{I} + \mathbf{S}.$$

4 Elemental stiffness and mass matrices

In this section, we outline the application of Algorithm 1 for the efficient computation of the mass and stiffness matrices appearing in (20).

4.1 Shape functions for the discrete space V_h

To construct the discrete space V_h we exploit the approach presented in [24], based on employing polynomial spaces defined over the bounding box of each element. More precisely, given an element $\kappa \in \mathcal{T}_h$, we first construct the Cartesian bounding box B_κ, such that $\overline{\kappa} \subset \overline{B_\kappa}$. Given $B_\kappa,\ \kappa \in \mathcal{T}_h$, it is easy to define a linear map between B_κ and the reference element $\hat{B} = (-1,1)^d$ as follow: $\mathbf{F}_\kappa : \hat{B} \to B_\kappa$ such that $\mathbf{F}_\kappa : \hat{\mathbf{x}} \in \hat{B} \longmapsto \mathbf{F}_\kappa(\hat{\mathbf{x}}) = \mathbf{J}_\kappa \hat{\mathbf{x}} + \mathbf{t}_\kappa$, where $\mathbf{J}_\kappa \in \mathbb{R}^{d\times d}$ is the Jacobi matrix of the transformation which describes the stretching in each direction, and $\mathbf{t}_\kappa \in \mathbb{R}^d$ is the translation between the point $\mathbf{0} \in \hat{B}$ and the baricenter of the bounded box B_κ, see Figure 6.

Remark 5. If $d = 2$ we can define the map $\mathbf{F}_\kappa : \hat{B} \to B_\kappa$ as follows: let $\mathbf{v}_i = \{(x_i, y_i)\}_{i=1}^4$ denote the coordinates of the four vertices of the box $B_\kappa \subset \mathbb{R}^2$, ordered in a counter clock-wise orientation, see Figure 6. The map $\mathbf{F}_\kappa$ is then identified by

$$\mathbf{J}_\kappa = \frac{1}{2}\begin{bmatrix} x_2 - x_1 & 0 \\ 0 & y_3 - y_1 \end{bmatrix}, \quad \mathbf{t}_\kappa = \frac{1}{2}\begin{bmatrix} x_1 + x_2 \\ y_1 + y_3 \end{bmatrix}.$$

We point out that since B_κ has edges which are aligned with the principal axes, the Jacobi matrix $\mathbf{J}_\kappa$ is diagonal, where $(\mathbf{J}_\kappa)_{1,1}$ and $(\mathbf{J}_\kappa)_{2,2}$ represent half of the size of base and the height of the box, respectively.

Employing the map $\mathbf{F}_\kappa,\ \kappa \in \mathcal{T}_h$, we may define a standard polynomial space $\mathcal{P}_p(B_\kappa)$ on B_κ spanned by a set of basis functions $\{\phi_{i,\kappa}\}$ for $i = 1, \ldots, N_{p_\kappa} = \dim(\mathcal{P}_p(B_\kappa))$. More precisely, we denote by $\{\mathcal{L}_n(x)\}_{n=0}^\infty$ the family of one–dimensional and L^2–orthonormal Legendre polynomials, defined over $L^2(-1,1)$, i.e.,

$$\mathcal{L}_n(x) = \frac{L_n(x)}{\|L_n\|_{L^2(-1,1)}}, \qquad \text{with} \;\; L_n(x) = \frac{1}{2^n n!}\frac{\mathrm{d}}{\mathrm{d}x}[(x^2-1)^n],$$

cf. [54, 39]. We then define the basis functions for the polynomial space $\mathcal{P}_p(\hat{B})$ as follows: writing $I = (i_1, i_2, \ldots, i_d)$ to denote the multi-index used to identify each basis function $\{\hat{\phi}_I\}_{0\le|I|\le p}$, where $|I| = i_1 + \cdots + i_d$, we have that

$$\hat{\phi}_I(\hat{\mathbf{x}}) = \hat{\phi}_I(\hat{x}_1, \ldots, \hat{x}_d) = \mathcal{L}_{i_1}(\hat{x}_1)\mathcal{L}_{i_2}(\hat{x}_2)\cdots\mathcal{L}_{i_d}(\hat{x}_d).$$

Then, the basis functions for the polynomial space $\mathcal{P}_{p_\kappa}(\kappa)$ are defined by using the map $\mathbf{F}_\kappa$, namely:

$$\phi_{I,\kappa}(\mathbf{x}) = \hat{\phi}_I(\mathbf{F}_\kappa^{-1}(\mathbf{x})) \quad \forall \mathbf{x} \in \kappa \subset B_\kappa \quad \forall I : 0 \le |I| \le p_\kappa. \tag{23}$$

The set $\{\phi_{I,\kappa} :\ 0 \le |I| \le p_\kappa,\ \kappa \in \mathcal{T}_h\}$ forms a basis for the space V_h. On each element $\kappa \in \mathcal{T}_h$ we introduce a bijective relation between the set of multi-indices $\{I = (i_1, \ldots, i_d) : 0 \le |I| \le p_\kappa\}$ and the set $\{1, 2, \ldots, N_{p_\kappa}\}$.

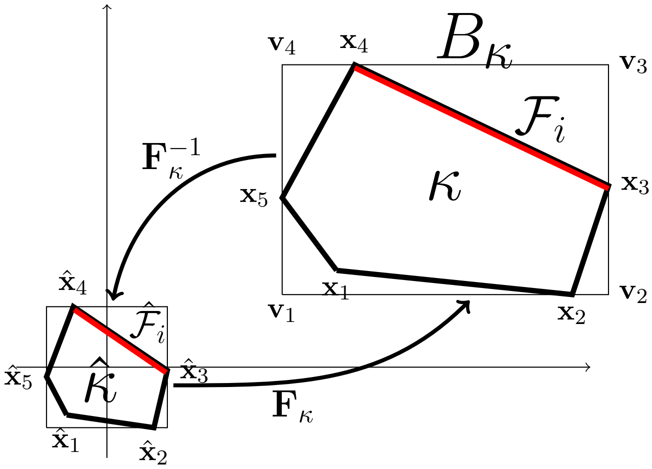

Figure 6: Example of a polygonal element $\kappa \in \mathcal{T}_h$, the relative bounded box B_κ, the map $\mathbf{F}_\kappa$ and $\hat{\kappa} = \mathbf{F}_\kappa^{-1}(\kappa)$.

4.2 Volume integrals over polytopic mesh elements

In the following we describe the application of Algorithm 1 to compute the entries in the local mass and element-based stiffness matrices

$$\mathbf{M}_{i,j}^{\kappa} = \int_\Omega \phi_{i,\kappa}\phi_{j,\kappa}\mathrm{d}\mathbf{x}, \quad \mathbf{V}_{i,j}^{\kappa} = \int_\Omega \nabla\phi_{i,\kappa}\cdot\nabla\phi_{j,\kappa}\mathrm{d}\mathbf{x} \quad i,j = 1,\dots,N_{p_\kappa}, \tag{24}$$

respectively, $\forall \kappa \in \mathcal{T}_h$. For simplicity of presentation, we restrict ourselves to two–dimensions, though we emphasize that the three–dimensional case is analogous, cf. Section 5.2 below. Since the basis functions are supported only on one element, employing the transformation $\mathbf{F}_\kappa$, we have

$$\mathbf{M}_{i,j}^{\kappa} = \int_\kappa \phi_{i,\kappa}(x,y)\phi_{j,\kappa}(x,y)\mathrm{d}\mathbf{x} = \int_{\hat{\kappa}} \hat{\phi}_i(\hat{x},\hat{y})\hat{\phi}_j(\hat{x},\hat{y})|\mathbf{J}_\kappa|\mathrm{d}\hat{\mathbf{x}}, \; i,j = 1,\dots,N_{p_\kappa},$$

where in the last integral $\hat{\kappa} = \mathbf{F}_\kappa^{-1}(\kappa) \subset \hat{B}$, see Figure 6. Here, the Jacobian of the transformation $\mathbf{F}_\kappa$ is given by $|\mathbf{J}_\kappa| = (\mathbf{J}_\kappa)_{1,1}(\mathbf{J}_\kappa)_{2,2}$, which is constant, due to the definition of the map, cf. Remark 5. In order to employ the *homogeneous function* integration method described in the previous section, we need to identify the coefficients of the homogeneous polynomial expansion for the function $\hat{\phi}_i(\hat{x},\hat{y})\hat{\phi}_j(\hat{x},\hat{y})$. We observe that $\hat{\phi}_i(\hat{x},\hat{y}) = \mathcal{L}_{i_1}(\hat{x})\mathcal{L}_{i_2}(\hat{y})$, and each one–dimensional Legendre polynomial can be expanded as

$$\mathcal{L}_{i_1}(\hat{x}) = \sum_{m=0}^{i_1} C_{i_1,m}\;\hat{x}^m, \qquad \mathcal{L}_{i_2}(\hat{y}) = \sum_{n=0}^{i_2} C_{i_2,n}\;\hat{y}^n. \tag{25}$$

Therefore, we have

$$\begin{aligned}
\mathbf{M}^{\kappa}_{i,j} &= \int_{\hat{\kappa}} \Big(\sum_{m=0}^{i_1} C_{i_1,m}\hat{x}^m\Big)\Big(\sum_{n=0}^{i_2} C_{i_2,n}\hat{y}^n\Big)\Big(\sum_{s=0}^{j_1} C_{j_1,s}\hat{x}^s\Big)\Big(\sum_{r=0}^{j_2} C_{j_2,r}\hat{y}^r\Big)|\mathbf{J}_\kappa|\mathrm{d}\hat{\mathbf{x}}\\
&= \int_{\hat{\kappa}} \Big(\sum_{k=0}^{i_1+j_1} \mathcal{C}_{i_1,i_2,k}\hat{x}^k\Big)\Big(\sum_{l=0}^{i_2+j_2} \mathcal{C}_{i_2,j_2,l}\hat{y}^l\Big)|\mathbf{J}_\kappa|\mathrm{d}\hat{\mathbf{x}}\\
&= \sum_{k=0}^{i_1+j_1}\sum_{l=0}^{i_2+j_2} \mathcal{C}_{i_1,j_1,k}\ \mathcal{C}_{i_2,j_2,l}\ |\mathbf{J}_\kappa| \int_{\hat{\kappa}} \hat{x}^k\hat{y}^l\mathrm{d}\hat{\mathbf{x}}\\
&= \sum_{k=0}^{i_1+j_1}\sum_{l=0}^{i_2+j_2} \mathcal{C}_{i_1,j_1,k}\ \mathcal{C}_{i_2,j_2,l}\ |\mathbf{J}_\kappa|\mathcal{I}(2,\hat{\kappa},k,l),
\end{aligned}$$

where the last identity follows from Algorithm 1, cf. Section 2. Here, we have written

$$\mathcal{C}_{i,j,k} = \sum_{n+m=k} (C_{i,n}\ C_{j,m}), \qquad \text{for } 0 \le i,j \le p_\kappa, \quad 0 \le k \le i+j. \tag{26}$$

Notice that the coefficients $\mathcal{C}_{i,j,k}$ can be evaluated, once and for all, independently of the polygonal element κ. We now consider the general element of the volume matrix $\mathbf{V}_{i,j}$, cf. (24). Proceeding as before, let $I,\ J$ be the two multi-indices corresponding respectively to i and j, we have

$$\mathbf{V}^{\kappa}_{i,j} = \int_\kappa \nabla\phi_i \cdot \nabla\phi_j\ \mathrm{d}\mathbf{x} = \underbrace{\int_\kappa \frac{\partial\phi_{I,\kappa}}{\partial x}\ \frac{\partial\phi_{J,\kappa}}{\partial x}\ \mathrm{d}\mathbf{x}}_{①} + \underbrace{\int_\kappa \frac{\partial\phi_{I,\kappa}}{\partial y}\ \frac{\partial\phi_{J,\kappa}}{\partial y}\ \mathrm{d}\mathbf{x}}_{②}. \tag{27}$$

Proceeding as before, we apply a change of variables to the terms ① and ② with respect to the map $\mathbf{F}_\kappa$; thereby, we obtain

$$① = \int_{\hat{\kappa}} \frac{\partial\phi_{I,\kappa}}{\partial x}(\mathbf{F}_\kappa(\hat{\mathbf{x}}))\frac{\partial\phi_{J,\kappa}}{\partial x}(\mathbf{F}_\kappa(\hat{\mathbf{x}}))|\mathbf{J}_\kappa|\mathrm{d}\hat{\mathbf{x}},$$

$$② = \int_{\hat{\kappa}} \frac{\partial\phi_{I,\kappa}}{\partial y}(\mathbf{F}_\kappa(\hat{\mathbf{x}}))\frac{\partial\phi_{J,\kappa}}{\partial y}(\mathbf{F}_\kappa(\hat{\mathbf{x}}))|\mathbf{J}_\kappa|\mathrm{d}\hat{\mathbf{x}}.$$

From the definition of $\mathbf{F}_\kappa$, the inverse map is given by $\mathbf{F}_\kappa^{-1}(\mathbf{x}) = \mathbf{J}_\kappa^{-1}(\mathbf{x} - \mathbf{t}_\kappa)$, cf. Remark 5. Then, using the definition (23) of the basis functions, we have the following characterization of the partial derivatives appearing in the terms ① and ②:

$$\frac{\partial}{\partial x}\phi_{I,\kappa}(\mathbf{x}) = \frac{\partial\hat{\phi}_I}{\partial\hat{x}}(\mathbf{F}_\kappa^{-1}(\mathbf{x}))\ (\mathbf{J}_\kappa^{-1})_{1,1}, \quad \frac{\partial}{\partial y}\phi_{I,\kappa}(\mathbf{x}) = \frac{\partial\hat{\phi}_I}{\partial\hat{y}}(\mathbf{F}_\kappa^{-1}(\mathbf{x}))\ (\mathbf{J}_\kappa^{-1})_{2,2}$$

where we have used that $(\mathbf{J}_\kappa^{-1})_{2,1} = (\mathbf{J}_\kappa^{-1})_{1,2} = 0$ since $\mathbf{J}_\kappa$ is diagonal. Then, ① can be written as:

$$① = \int_{\hat{\kappa}} \frac{\partial\hat{\phi}_I}{\partial\hat{x}}(\hat{\mathbf{x}})\frac{\partial\hat{\phi}_J}{\partial\hat{x}}(\hat{\mathbf{x}})\ (\mathbf{J}_\kappa^{-1})^2_{1,1}|\mathbf{J}_\kappa|\mathrm{d}\hat{\mathbf{x}}.$$

Since $(\mathbf{J}_\kappa^{-1})^2_{1,1}|\mathbf{J}_\kappa|$ is constant, the integrand function of term ① is a polynomial. Thereby, we have the following relation:

$$\left.\begin{aligned}
\frac{\partial\hat{\phi}_I}{\partial\hat{x}}(\hat{\mathbf{x}}) &= \mathcal{L}'_{i_1}(\hat{x})\ \mathcal{L}_{i_2}(\hat{y}),\\
\frac{\partial\hat{\phi}_J}{\partial\hat{x}}(\hat{\mathbf{x}}) &= \mathcal{L}'_{j_1}(\hat{x})\ \mathcal{L}_{j_2}(\hat{y}),
\end{aligned}\right\} \Rightarrow \frac{\partial\hat{\phi}_I}{\partial\hat{x}}(\hat{\mathbf{x}})\frac{\partial\hat{\phi}_J}{\partial\hat{x}}(\hat{\mathbf{x}}) = \mathcal{L}'_{i_1}(\hat{x})\ \mathcal{L}_{i_2}(\hat{y})\ \mathcal{L}'_{j_1}(\hat{x})\ \mathcal{L}_{j_2}(\hat{y}).$$

From the expansion (25) of the Legendre polynomials, we note that

$$\mathcal{L}_0'(\hat{x}) = 0, \qquad \mathcal{L}_i'(\hat{x}) = \sum_{m=0}^{i-1} (m+1) C_{i,m+1}\ \hat{x}^m = \sum_{m=0}^{i-1} C'_{i,m}\ \hat{x}^m, \quad \text{for } i > 0; \tag{28}$$

where the indices $C'_{i,m} = (m+1)C_{i,m+1}$ are the coefficients for the expansion of $\mathcal{L}_i'(\cdot)$. We deduce that ① $= 0$ if $i_1 = 0$ or $j_1 = 0$, and

$$① = \sum_{k=0}^{i_1+j_1-2} \sum_{l=0}^{i_2+j_2} \mathcal{C}'_{i_1,i_2,k}\ \mathcal{C}_{i_2,j_2,l}\ (\mathbf{J}_\kappa^{-1})^2_{1,1} |\mathbf{J}_\kappa| \int_{\hat{\kappa}} \hat{x}^k \hat{y}^l \mathrm{d}\hat{\mathbf{x}}, \quad i_1, j_1 > 0,$$

where $\mathcal{C}_{i_2,j_2,l}$ is defined in (26), and

$$\mathcal{C}'_{i,j,k} = \sum_{n+m=k} C'_{i,n}\ C'_{j,m}, \quad 1 \le i, j \le p_\kappa, \text{ for } 0 \le k \le i+j-2,$$

with $C'_{i,n} = (n+1)C_{i,n+1}$, $C'_{j,m} = (m+1)C_{j,m+1}$, cf. (28), is the expansion of the derivatives of the Legendre polynomials which is computable independently of the element κ, $\kappa \in \mathcal{T}_h$. Analogously, we deduce the following expression for the second term of equation (27):

$$② = \sum_{k=0}^{i_1+j_1} \sum_{l=0}^{i_2+j_2-2} \mathcal{C}_{i_1,i_2,k}\ \mathcal{C}'_{i_2,j_2,l}\ (\mathbf{J}_\kappa^{-1})^2_{2,2} |\mathbf{J}_\kappa| \int_{\hat{\kappa}} \hat{x}^k \hat{y}^l \mathrm{d}\hat{\mathbf{x}}.$$

4.3 Interface integrals over polytopic mesh elements

With regards the interface integrals appearing in the equation (18), we describe the method by expanding the jump and average operators and computing each term separately, working, for simplicity, again in two–dimensions. Firstly, however, we discuss how to transform the integral over a physical face $F \subset \partial\kappa$ to the corresponding integral over the face $\hat{F} = \mathbf{F}_\kappa^{-1}(F) \subset \partial\hat{\kappa}$ on the reference rectangular element $\hat{\kappa}$. To this end, let $F \subset \partial\kappa$ be a face of the polygon κ, $\kappa \in \mathcal{T}_h$, and let $\mathbf{x}_1 = (x_1, y_1)$ and $\mathbf{x}_2 = (x_2, y_2)$ denote the vertices of the face, based on counter clock-wise ordering of the polygon vertices. The face $\hat{F} = \mathbf{F}_\kappa^{-1}(F)$ is identified by the two vertices $\hat{\mathbf{x}}_1 = \mathbf{F}_\kappa^{-1}(\mathbf{x})$ and $\hat{\mathbf{x}}_2 = \mathbf{F}_\kappa^{-1}(\mathbf{x}_2)$. For a general integrable function $g : \kappa \to \mathbb{R}$ we have

$$\int_F g(x,y) \mathrm{d}\sigma(x,y) = \int_{\hat{F}} g(\mathbf{F}_\kappa(\hat{x},\hat{y}))\ \mathrm{d}\sigma(\mathbf{F}_\kappa(\hat{x},\hat{y})),$$

where $\mathrm{d}\sigma(\mathbf{F}_\kappa(\hat{x},\hat{y})) = \mathcal{J}_F\ \mathrm{d}\hat{\sigma}$ and $\mathcal{J}_F$ is defined as $\mathcal{J}_F = \|\mathbf{J}_\kappa^{-\top} \hat{\mathbf{n}}_{\hat{F}}\| |\mathbf{J}_\kappa|$, where $\hat{\mathbf{n}}_{\hat{F}}$ is the unit outward normal vector to $\hat{F}$.

We next describe how to compute the interface integrals. From the definition of the jump and average operators, cf. (17), on each edge $F \in \mathcal{F}_h^I$ shared by the elements $\kappa^\pm$ we need to assemble

$$\begin{aligned}
\mathbf{S}_{i,j}^{+/+} &= \int_F \alpha_h\ \phi_{i,\kappa^+}\ \phi_{j,\kappa^+}\ \mathrm{d}\sigma, & \mathbf{I}_{i,j}^{+/+} &= \frac{1}{2} \int_F (\nabla\phi_{i,\kappa^+} \cdot \mathbf{n}^+)\ \phi_{j,\kappa^+}\ \mathrm{d}\sigma, \\
\mathbf{S}_{i,j}^{-/-} &= \int_F \alpha_h\ \phi_{i,\kappa^-}\ \phi_{j,\kappa^-}\ \mathrm{d}\sigma, & \mathbf{I}_{i,j}^{-/-} &= \frac{1}{2} \int_F (\nabla\phi_{i,\kappa^-} \cdot \mathbf{n}^-)\ \phi_{j,\kappa^-}\ \mathrm{d}\sigma, \\
\mathbf{S}_{i,j}^{+/-} &= -\int_F \alpha_h\ \phi_{i,\kappa^+}\ \phi_{j,\kappa^-}\ \mathrm{d}\sigma, & \mathbf{I}_{i,j}^{+/-} &= -\frac{1}{2} \int_F (\nabla\phi_{i,\kappa^+} \cdot \mathbf{n}^+)\ \phi_{j,\kappa^-}\ \mathrm{d}\sigma, \\
\mathbf{S}_{i,j}^{-/+} &= -\int_F \alpha_h\ \phi_{i,\kappa^-}\ \phi_{j,\kappa^+}\ \mathrm{d}\sigma, & \mathbf{I}_{i,j}^{-/+} &= -\frac{1}{2} \int_F (\nabla\phi_{i,\kappa^-} \cdot \mathbf{n}^-)\ \phi_{j,\kappa^+}\ \mathrm{d}\sigma,
\end{aligned}$$

for $i, j = 1, \dots, N_{p_{\kappa^\pm}}$. Analogously, on the boundary face $F \in \mathcal{F}_h^B$ belonging to $\kappa^+ \in \mathcal{T}_h$ we only have to compute

$$\mathbf{S}_{i,j}^{+/+} = \int_F \alpha_h \ \phi_{i,\kappa^+} \ \phi_{j,\kappa^+} \ \mathrm{d}\sigma, \qquad \mathbf{I}_{i,j}^{+/+} = \int_F (\nabla \phi_{i,\kappa^+} \cdot \mathbf{n}^+) \ \phi_{j,\kappa^+} \ \mathrm{d}\sigma,$$

for $i, j = 1, \dots, N_{p_{\kappa^+}}$. We next show how to efficiently compute a term of the form

$$\mathbf{S}_{i,j}^{+/+} = \int_F \alpha_h \ \phi_{I,\kappa^+}(x,y) \ \phi_{J,\kappa^+}(x,y) \mathrm{d}\sigma,$$

where I, J are the suitable multi-indices associated to $i, j = 1, \dots, N_{p_{\kappa^+}}$, respectively. Proceeding as before, we have

$$\begin{aligned} \mathbf{S}_{i,j}^{+/+} &= \int_F \alpha_h \phi_{I,\kappa^+}(x,y) \phi_{J,\kappa^+}(x,y) \mathrm{d}\sigma(x,y) = \int_{\hat{F}} \alpha_h \hat{\phi}_I(\hat{x},\hat{y}) \hat{\phi}_J(\hat{x},\hat{y}) \mathcal{J}_F \mathrm{d}\hat{\sigma} \\ &= \sum_{k=0}^{i_1+j_1} \sum_{l=0}^{i_2+j_2} \alpha_h \ \mathcal{C}_{i_1,j_1,k} \ \mathcal{C}_{i_2,j_2,l} \ \mathcal{J}_F \int_{\hat{F}} \hat{x}^k \hat{y}^l \mathrm{d}\hat{\sigma}, \end{aligned}$$

where the integral of bivariates is computed as $\int_{\hat{F}} \hat{x}^k \hat{y}^l \mathrm{d}\hat{\sigma} = \mathcal{I}(1, \hat{F}, k, l)$. Analogously, we have

$$\begin{aligned} \mathbf{S}_{i,j}^{+/-} &= -\int_F \alpha_h \ \phi_{I,\kappa^+}(x,y) \phi_{J,\kappa^-}(x,y) \mathrm{d}\sigma(x,y) \\ &= -\int_{\mathbf{F}_{\kappa^+}^{-1}(F)} \alpha_h \underbrace{\phi_{I,\kappa^+}(\mathbf{F}_{\kappa^+}(\hat{\mathbf{x}}))}_{ⓐ} \underbrace{\phi_{J,\kappa^-}(\mathbf{F}_{\kappa^+}(\hat{\mathbf{x}}))}_{ⓑ} \mathcal{J}_{F^+} \mathrm{d}\sigma. \end{aligned} \tag{29}$$

For the term ⓐ, we directly apply the definition of the basis function, and obtain

$$ⓐ = \phi_{I,\kappa^+}(\mathbf{F}_{\kappa^+}(\hat{\mathbf{x}})) = \hat{\phi}_I(\mathbf{F}_{\kappa^+}^{-1}(\mathbf{F}_{\kappa^+}(\hat{\mathbf{x}}))) = \hat{\phi}_I(\hat{\mathbf{x}}) = \sum_{k=0}^{i_1} \sum_{l=0}^{i_2} C_{i_1,k} \ C_{i_2,l} \ \hat{x}^k \hat{y}^l, \tag{30}$$

while for the term ⓑ we have

$$ⓑ = \phi_{J,\kappa^-}(\mathbf{F}_{\kappa^+}(\hat{\mathbf{x}})) = \hat{\phi}_J(\mathbf{F}_{\kappa^-}^{-1}(\mathbf{F}_{\kappa^+}(\hat{\mathbf{x}}))).$$

In order to obtain a homogeneous polynomial expansion for ⓑ we have to write explicitly the composite map $\tilde{\mathbf{F}}(\hat{\mathbf{x}}) = \mathbf{F}_{\kappa^-}^{-1}(\mathbf{F}_{\kappa^+}(\hat{\mathbf{x}}))$. That is

$$\tilde{\mathbf{F}}(\hat{\mathbf{x}}) = \mathbf{J}_{\kappa^-}^{-1}(\mathbf{J}_{\kappa^+}\hat{\mathbf{x}} + \mathbf{t}_{\kappa^+}) - \mathbf{J}_{\kappa^-}^{-1}\mathbf{t}_{\kappa^-} = \underbrace{\mathbf{J}_{\kappa^-}^{-1}\mathbf{J}_{\kappa^+}}_{\tilde{\mathbf{J}}} \hat{\mathbf{x}} + \underbrace{\mathbf{J}_{\kappa^-}^{-1}(\mathbf{t}_{\kappa^+} - \mathbf{t}_{\kappa^-})}_{\tilde{\mathbf{t}}},$$

where the matrix $\tilde{\mathbf{J}}$ is diagonal since $\mathbf{J}_{\kappa^-}^{-1}$ and $\mathbf{J}_{\kappa^+}$ are diagonal. We then have

$$\begin{aligned} ⓑ &= \hat{\phi}_J(\hat{\mathbf{F}}(\hat{\mathbf{x}})) = \hat{\phi}_J(\tilde{\mathbf{J}}\hat{\mathbf{x}} + \tilde{\mathbf{t}}) = \hat{\phi}_J(\tilde{\mathbf{J}}_{1,1}\hat{x} + \tilde{\mathbf{t}}_1, \tilde{\mathbf{J}}_{2,2}\hat{y} + \tilde{\mathbf{t}}_2) \\ &= \sum_{k=0}^{j_1} \sum_{l=0}^{j_2} C_{j_1,k} \ C_{j_2,l} \ (\tilde{\mathbf{J}}_{1,1}\hat{x} + \tilde{\mathbf{t}}_1)^k (\tilde{\mathbf{J}}_{2,2}\hat{y} + \tilde{\mathbf{t}}_2)^l. \end{aligned} \tag{31}$$

Combining (30) and (31), and denoting by $\hat{F}^+ = \mathbf{F}_{\kappa^+}^{-1}(F)$, cf. Figure 7, from (29) we obtain

$$\mathbf{S}_{i,j}^{+/-} = -\sum_{k=0}^{i_1+j_1} \sum_{l=0}^{i_2+j_2} \tilde{\mathcal{X}}_{i_1,j_1,k} \ \tilde{\mathcal{Y}}_{i_2,j_2,l} \ \mathcal{J}_{F^+} \int_{\hat{F}^+} \hat{x}^k \hat{y}^l \mathrm{d}\hat{\sigma},$$

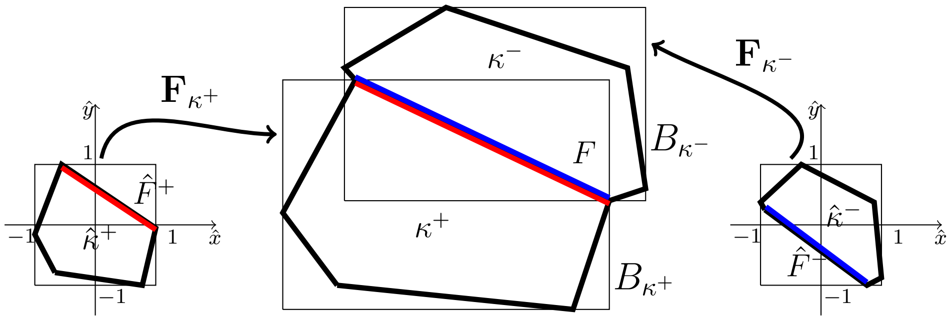

Figure 7: Example of a polygonal elements $\kappa^{\pm} \in \mathcal{T}_h$, together with the bounded boxes $B_{\kappa^{\pm}}$, and the local maps $\mathbf{F}_{\kappa^{\pm}} : \hat{\kappa} \to \kappa^{\pm}$ for the common face $F \subset \kappa^{\pm}$.

where $\tilde{\mathcal{X}}$ and $\tilde{\mathcal{Y}}$ are defined as

$$\left.\begin{aligned} \tilde{\mathcal{X}}_{i,j,k} &= \sum_{n+m=k} (C_{i,n}\ \tilde{X}_{j,m}) \\ \tilde{\mathcal{Y}}_{i,j,k} &= \sum_{n+m=k} (C_{i,n}\ \tilde{Y}_{j,m}) \end{aligned}\right\} \quad \text{for } 0 \le i \le p_{\kappa^+},\ 0 \le j \le p_{\kappa^-},\ 0 \le k \le i+j.$$

Here, as before, $C_{i,n}$ are the coefficients of the homogeneous function expansion of the Legendre polynomials in $(-1,1)$, while $\tilde{X}_{j,m}$ and $\tilde{Y}_{j,m}$ are defined by

$$\left.\begin{aligned} \tilde{X}_{j,m} &= \sum_{r=m}^{j} C_{j,r} \begin{pmatrix} r \\ m \end{pmatrix} (\tilde{\mathbf{J}}_{1,1})^m\ (\tilde{\mathbf{t}}_1)^{r-m} \\ \tilde{Y}_{j,m} &= \sum_{r=m}^{j} C_{j,r} \begin{pmatrix} r \\ m \end{pmatrix} (\tilde{\mathbf{J}}_{2,2})^m\ (\tilde{\mathbf{t}}_2)^{r-m} \end{aligned}\right\} \quad \text{for } 0 \le j \le p_{\kappa^-},\ j \le m \le p_{\kappa^-};$$

here, we have exploited the Newton-binomial expansion of the terms $(\tilde{\mathbf{J}}_{1,1}\hat{x} + \tilde{\mathbf{t}}_1)^k$ and $(\tilde{\mathbf{J}}_{2,2}\hat{y} + \tilde{\mathbf{t}}_2)^l$ appearing in equation (31).

Similar considerations allow us to compute

$$\begin{aligned} \mathbf{I}_{i,j}^{+/+} &= \frac{1}{2}\Big(\int_F \frac{\partial \phi_{I,\kappa^+}}{\partial x}(x,y)\phi_{J,\kappa^+}(x,y)n_x^+ + \int_F \frac{\partial \phi_{I,\kappa^+}}{\partial y}(x,y)\phi_{J,\kappa^+}(x,y)n_y^+\Big) \\ &= \frac{1}{2}\Big(\int_{\hat{F}} (\mathbf{J}_{\kappa^+}^{-1})_{1,1}\frac{\partial \hat{\phi}_I}{\partial \hat{x}}\hat{\phi}_J n_x^+ \mathcal{J}_F \mathrm{d}\hat{\sigma} + \int_{\hat{F}} (\mathbf{J}_{\kappa^+}^{-1})_{2,2}\frac{\partial \hat{\phi}_I}{\partial \hat{y}}\hat{\phi}_J n_y^+ \mathcal{J}_F \mathrm{d}\hat{\sigma}\Big) \\ &= \frac{1}{2}\mathcal{J}_F\Big((\mathbf{J}_{\kappa^+}^{-1})_{1,1} n_x^+ \sum_{k=0}^{i_1+j_1-1}\ \sum_{l=0}^{i_2+j_2} \mathcal{C}''_{i_1,i_2,k}\mathcal{C}_{i_2,j_2,l}\int_{\hat{F}} \hat{x}^k\hat{y}^l \mathrm{d}\hat{\sigma}\ +\ \dots \\ &\qquad \dots\ +\ (\mathbf{J}_{\kappa^+}^{-1})_{2,2} n_y^+ \sum_{k=0}^{i_1+j_1}\ \sum_{l=0}^{i_2+j_2-1} \mathcal{C}_{i_1,i_2,k}\ \mathcal{C}''_{i_2,j_2,l}\int_{\hat{F}} \hat{x}^k\hat{y}^l \mathrm{d}\hat{\sigma}\Big), \end{aligned}$$

where $\mathcal{C}''_{i,j,k}$ are defined as

$$\begin{cases} \mathcal{C}''_{0,j,k} = 0 & \forall j,\ \forall k, \\ \mathcal{C}''_{i,j,k} = \sum_{n+m=k} C'_{i,n} C_{j,m}, & 1 \le i \le p_{\kappa^+}, 0 \le j \le p_{\kappa^+}, 0 \le k \le i+j-1, \end{cases}$$

and where $\mathbf{n}^+ = [n_x^+, n_y^+]^\top$ is the unit outward normal vector to the physical face F from

κ^+. Similarly,

$$\begin{aligned}
\mathbf{I}_{i,j}^{+/-} &= -\frac{1}{2}\int_F (\nabla\phi_{I,\kappa^+}\cdot\mathbf{n}^+)\phi_{J,\kappa^-}\mathrm{d}\sigma \\
&= -\frac{1}{2}\Big(\int_F \frac{\partial\phi_{I,\kappa^+}}{\partial x}\phi_{J,\kappa^-}n_x^+\mathrm{d}\sigma + \int_F \frac{\partial\phi_{I,\kappa^+}}{\partial y}\phi_{J,\kappa^-}n_y^+\mathrm{d}\sigma\Big) \\
&= -\frac{1}{2}\mathcal{J}_F\Big((\mathbf{J}_\kappa^{-1})_{1,1}\sum_{k=0}^{i_1+j_1-1}\sum_{l=0}^{i_2+j_2}\tilde{\mathcal{X}}'_{i_1,i_2,k}\tilde{\mathcal{Y}}_{i_2,j_2,l}\int_{\hat{F}^+}\hat{x}^k\hat{y}^l\mathrm{d}\hat{\sigma} \ + \ \ldots \\
&\qquad \ldots \ + \ (\mathbf{J}_\kappa^{-1})_{2,2}\sum_{k=0}^{i_1+j_1}\sum_{l=0}^{i_2+j_2-1}\tilde{\mathcal{X}}_{i_1,i_2,k}\ \tilde{\mathcal{Y}}'_{i_2,j_2,l}\int_{\hat{F}^+}\hat{x}^k\hat{y}^l\mathrm{d}\hat{\sigma}\Big),
\end{aligned}$$

where we have also introduced $\tilde{\mathcal{X}}'$ and $\tilde{\mathcal{Y}}'$ defined as

$$\left.\begin{aligned}
\tilde{\mathcal{X}}'_{i,j,k} &= \sum_{n+m=k}(C'_{i,n}\ \tilde{X}_{j,m}),\\
\tilde{\mathcal{Y}}'_{i,j,k} &= \sum_{n+m=k}(C'_{i,n}\ \tilde{Y}_{j,m}),
\end{aligned}\right\}\ \text{for } 1\le i\le p_{\kappa^+},\ 0\le j\le p_{\kappa^-},\ 0\le k\le i+j-1.$$

Remark 6. The coefficients $\tilde{X}$ and $\tilde{Y}$ depend on the maps $\mathbf{F}_{\kappa^+}$ and $\mathbf{F}_{\kappa^-}$, as well as $\tilde{\mathcal{X}}$, $\tilde{\mathcal{X}}'$, $\tilde{\mathcal{Y}}$ and $\tilde{\mathcal{Y}}'$; thereby, they must be computed for each element κ in the mesh $\mathcal{T}_h$.
Remark 7. With regards the computation of the forcing term

$$\mathbf{f}_i = \int_\Omega f(\mathbf{x})\phi_i(\mathbf{x})\mathrm{d}\mathbf{x},\ \forall i=1,\ldots,N_h, \tag{32}$$

we point out that the quadrature method proposed in this paper allows to exactly evaluate (32) when f is a constant or a polynomial function. If f is a general function, an explicit polynomial approximation of f is required.

5 Numerical experiments

We present some two– and three–dimensional numerical experiments to test the practical performance of the proposed approach. Here, the results are compared with standard assembly algorithms based on employing Gaussian quadrature rules on a sub-tessellation.

5.1 Two–dimensional test case

We test the performance of the algorithm outlined in Section 4 for the computation of the elemental mass and stiffness matrices resulting from the DG discretization (19) on Voronoi decompositions as shown in Fig. 8. In particular, we compare the CPU-time needed to assemble the local and global elemental matrices using Agorithm 1, cf. Section 4, with classical *Gaussian Quadrature Integration* over polygonal domains, based on the *Sub-tessellation* method on polygons and *Gaussian line integration* for the related interface terms. More precisely, given $\kappa\in\mathcal{T}_h$, the *Sub-Tessellation* scheme on κ is performed by constructing a non-overlapping sub-tessellation $\kappa_{\mathscr{S}}=\{\tau_\kappa\}$ consisting of standard triangular elements; in particular, as, for our tests, we consider Voronoi numerical grids, we exploit the convexity of κ and define $\kappa_{\mathscr{S}}$ by connecting the centre of mass of κ with its

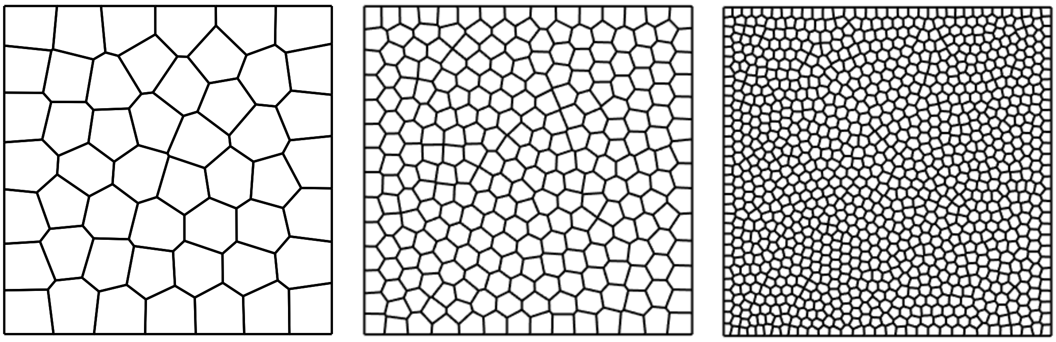

(a) 50 elements. (b) 250 elements. (c) 1000 elements.

Figure 8: Example of Voronoi mesh on $\Omega = (0,1)^2$.

vertices. As an example, if we consider computing the elemental mass matrix $\mathbf{M}^{\kappa}_{i,j}$, we have that

$$\mathbf{M}^{\kappa}_{i,j} = \int_{\kappa} \phi_i \phi_j \mathrm{d}\mathbf{x} \approx \sum_{\tau_\kappa \in \kappa_{\mathscr{S}}} \sum_{r=1}^{q_{\tau_\kappa}} \phi_i(\mathbf{F}_{\tau_\kappa}(\boldsymbol{\xi}_r)) \phi_j(\mathbf{F}_{\tau_\kappa}(\boldsymbol{\xi}_r)) |\mathbf{J}_{\tau_\kappa}| \omega_r,$$

where $\mathbf{F}_{\tau_\kappa} : \hat{\tau} \to \tau_\kappa$ is the mapping from the reference simplex $\hat{\tau}$ to τ_κ, with Jacobian $|\mathbf{J}_{\tau_\kappa}|$, and $\{(\boldsymbol{\xi}_r, \omega_r)\}_{r=1}^{q_\kappa}$ denotes the quadrature rule defined on $\hat{\tau}$. The construction of quadrature rules on $\hat{\tau}$ may be computed based on employing the Duffy transformation, whereby the reference tensor-product element $(-1,1)^2$ is mapped to the reference simplex. As the algorithm outlined in Section 4 does not require the definition of quadrature nodes and weights, in the following we will refer to it as the *Quadrature Free Method.* Consider the problem (19) introduced in Section 3 with $d = 2$ and $\Omega = (0,1)^2$, where we select the set of basis functions $\{\phi_i\}_{i=1}^{N_h}$ for V_h as described in Section 4. In order to quantify the performance of the proposed approach, we consider a series of numerical tests obtained by varying the polynomial degree $p_\kappa = p$ for all $\kappa \in \mathcal{T}_h$, between 1 and 6 and by employing a series of uniform polygonal meshes of different granularity, cf. Figure 8. The numerical grids are constructed based on employing `PolyMesher`, cf. [62]. Here, we are interested in the CPU time needed to assemble the matrices (21) and (22).

In the first test case, we consider the CPU time needed to assemble the matrices $\mathbf{M}$ and $\mathbf{V}$. As pointed out in Section 4, these matrices are block diagonal and each block consists of an integral over each polygonal element $\kappa \in \mathcal{T}_h$. In Figure 9 we present the comparison between the CPU times needed to assemble the global matrices $\mathbf{M}$ and $\mathbf{V}$ based on employing the *Quadrature Free Method* and *Gaussian Quadrature Integration* when varying the number of elements $N_e \in \{64, 256, 1024, 4094, 16384, 65536\}$ and the polynomial degree $p \in \{1,2,3\}$ (left), and $p \in \{4,5,6\}$ (right). Clearly, our approach outperforms the classical *Sub-tessellation* method leading to substantial gains in efficiency. For a more detailed comparison, we have presented in Figure 11(a) the logarithmic-scaled graphs of each computation: from the results of Figure 11(a) we observe that the CPU time grows like $\mathcal{O}(N_e)$, as N_e increases, as expected.

We have repeated the same set of numerical experiments measuring the CPU times needed to assemble the face terms appearing in the matrices $\mathbf{S}$ and $\mathbf{I}$; these results are reported in Figure 10. Here, the domains of integration of the integrals involved are the edges of the polygonal elements, which are simply line segments in the plane $\mathbf{R}^2$. Here, we compare the *Quadrature Free Method* method described in Section 4.3 with classical *Gaussian Line Integration*, where the integrating function is pointwise evaluated on the physical

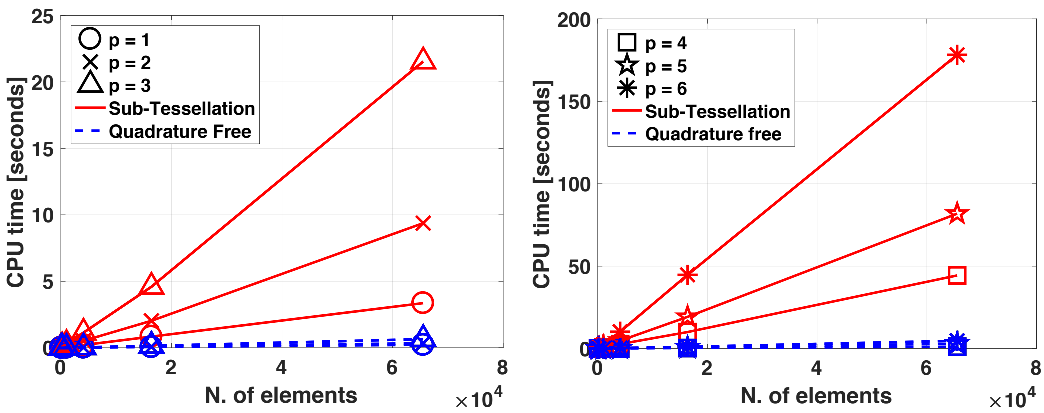

(a) Comparison for $p \in \{1, 2, 3\}$. (b) Comparison for $p \in \{4, 5, 6\}$.

Figure 9: Comparison of the CPU time needed to assemble the global matrices $\mathbf{M}$ and $\mathbf{V}$ for a two–dimensional problem by using the proposed *Quadrature Free Method* and the classical *Sub-Tessellation* scheme. For each algorithm, each line is obtained by fixing the polynomial approximation degree $p \in \{1, 2, 3\}$ (left) and $p \in \{4, 5, 6\}$ (right), and measuring the CPU time by varying the number of elements in the underlying mesh.

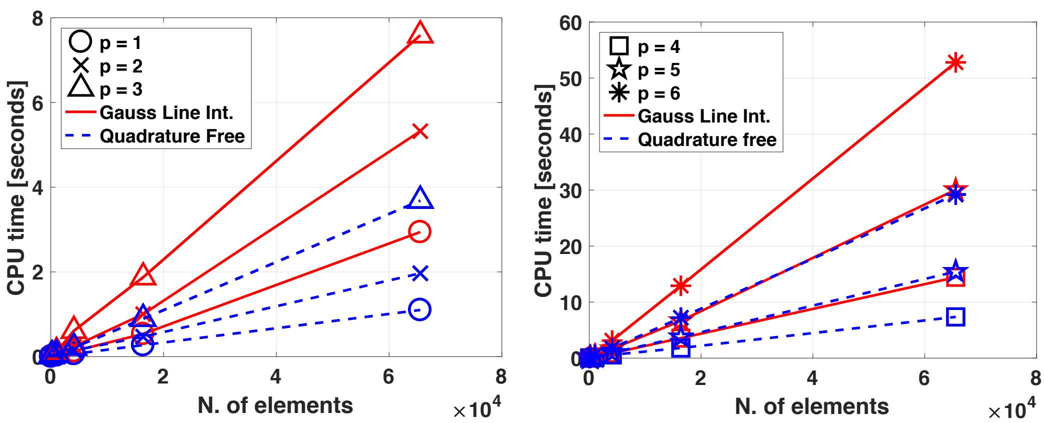

(a) Comparison for $p \in \{1, 2, 3\}$. (b) Comparison for $p \in \{4, 5, 6\}$.

Figure 10: Comparison of the CPU time needed to assemble the global matrices $\mathbf{S}$ and $\mathbf{I}$ for a two–dimensional problem by using the proposed *Quadrature Free Method* and the classical *Gauss Line Integration* scheme. For each approach, each line is obtained by fixing the polynomial approximation degree $p \in \{1, 2, 3\}$ (left) and $p \in \{4, 5, 6\}$ (right), and measuring the CPU time by varying the number of elements in the underlying mesh.

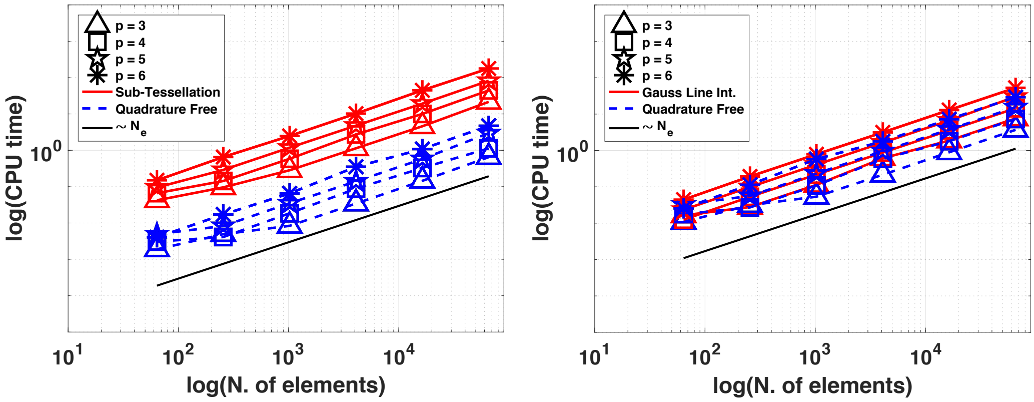

(a) CPU time comparison needed to assemble **M** and **V** in log-log scale.

(b) CPU time comparison needed to assemble **S** and **I** in log-log scale.

Figure 11: Comparison between the CPU time needed by the two method to assemble the global matrices **M** and **V** (left) and **S** and **I** (right) for a three–dimensional problem, versus the number of elements and for different choices of $p = 3, \ldots, 6$ (log-log scale).

numerical nodes lying on each face. The graphs in Figure 10(a) and 10(b) show the comparison between the CPU time taken for the two different approaches. Here, we again observe that significant computational savings are made when the proposed *Quadrature Free Method* is employed, though the increase in efficiency is less than that attained for the computation of the volume integrals. In Figure 11(b) we plot the logarithmic-scaled time growing with respect to the number of mesh elements; again the CPU time grows as $\mathcal{O}(N_e)$ as N_e increases.

Referring to Figures 9 and 10, we observe that the cost of assembly of the matrices **M** and **V**, which involve volume integrals over each element κ in the computational mesh $\mathcal{T}_h$, is more expensive than the time it takes to assemble the face-baced matrices **S** and **I**, when the classical *Gaussian Line Integration* method is employed. This is, of course, due to the greater number of function evaluations required to compute **M** and **V** on the underlying sub-tessellation; note that in two–dimensions, a sub-tesellation of the faces is not necessary, since they simply consist of line segments. However, the opposite behaviour is observed when the *Quadrature Free Method* is employed; in this case, the volume integrals can be very efficiently computed since the coefficients $\mathcal{C}_{i,j,k}$ and $\mathcal{C}'_{i,j,k}$ only need to be computed once, cf. Section 4.2. On the other hand, computing the face integrals present in **S** and **I** requires the evaluation of the coefficients $\tilde{X}_{b,m}$, $\tilde{\mathcal{X}}_{a,b,k}$, $\tilde{\mathcal{X}}'_{a,b,k}$, $\tilde{Y}_{b,m}$, $\tilde{\mathcal{Y}}_{a,b,k}$, and $\tilde{\mathcal{Y}}'_{a,b,k}$, cf. Section 4.3, which must be computed for each face $F \in \mathcal{F}_h$.

5.2 Three–dimensional test case

We now consider the diffusion-reaction problem (19) with $d = 3$ and $\Omega = (0,1)^3$. The polyhedral grids employed for this test case are defined by agglomeration: starting from a fine partition $\mathcal{T}_{fine}$ of Ω consisting of N_{fine} disjoint tetrahedrons $\{\kappa_f^i\}_{i=1}^{N_{fine}}$, such that $\overline{\Omega} = \cup_{i=1}^{N_{fine}} \overline{\kappa}_f^i$, a coarse mesh $\mathcal{T}_h$ of Ω consisting of disjoint polyhedral elements κ can be defined such that

$$\kappa = \cup_{\kappa'_f \in \mathscr{S}_\kappa} \kappa'_f \quad \forall \kappa \in \mathcal{T}_h, \tag{33}$$

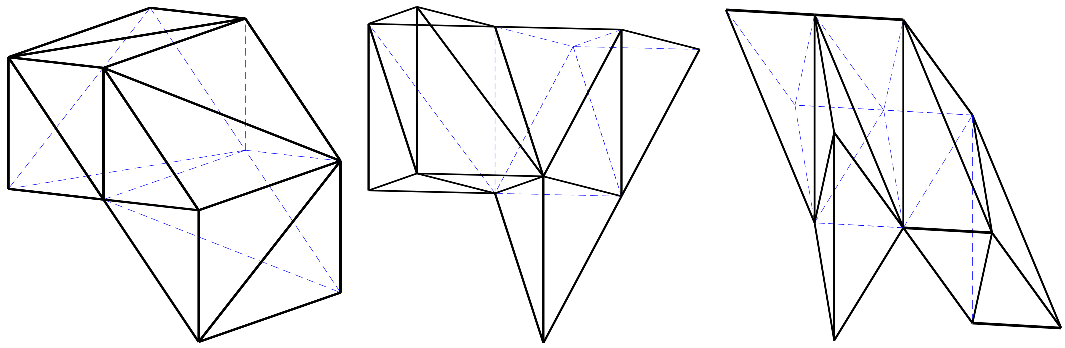

(a) Element κ_1. (b) Element κ_2. (c) Element κ_3.

Figure 12: Example of polyhedral elements $\kappa \in \mathcal{T}_h$ obtained by agglomeration of tetrahedrons. κ_1 has 18 triangular *faces*, κ_2 has 20 triangular *faces* and κ_3 has 22 triangular *faces*.

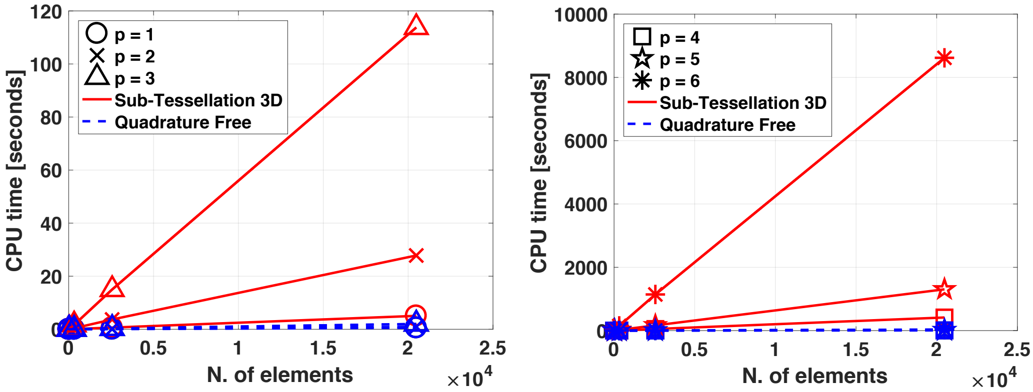

(a) Comparison for $p \in \{1, 2, 3\}$. (b) Comparison for $p \in \{4, 5, 6\}$.

Figure 13: Comparison of the CPU time needed to assemble the global matrices $\mathbf{M}$ and $\mathbf{V}$ for a three–dimensional problem by using the proposed *Quadrature Free Method* and the classical *Sub-Tessellation* method. For each approach, each line is obtained by fixing the polynomial approximation degree $p \in \{1, 2, 3\}$ (left) and $p \in \{4, 5, 6\}$ (right), and measuring the CPU time by varying the number of elements of the underlying mesh.

where $\mathscr{S}_\kappa \subset \mathcal{T}_h^{fine}$ denotes the set of fine elements which forms κ. Here, the agglomeration of fine tetrahedral elements is performed based on employing the *METIS* library for graph partitioning, cf., for example, [44, 45]. With this definition each polyhedral element is typically non-convex. For simplicity, we have considered only the case of simply connected elements. In this particular case, the faces of the mesh $\mathcal{T}_h$ are the triangular intersections of two–dimensional facets of neighbouring elements. Figure 12 shows three examples of the polyhedral elements resulting from agglomeration.

We perform a similar set of experiments as the ones outlined in Section 5.2 for the two–dimensional case. Again, we compare the CPU time required by the proposed *Quadrature Free Mehod* with the classical *Gaussian Quadrature Integration* approach to assemble the stiffness and mass matrices resulting from the DG discretization of problem (19). Numerical integration over a polyhedral domain is required to assemble the matrices $\mathbf{M}$ and $\mathbf{V}$, cf. (21), whereas for the computation of $\mathbf{S}$ and $\mathbf{I}$, cf. (22), a cubature rule over polygonal faces (here triangular shaped) is needed. In general, for three–dimensional problems the classical *Gaussian Quadrature Integration* approach consists in the application of the *Sub-*

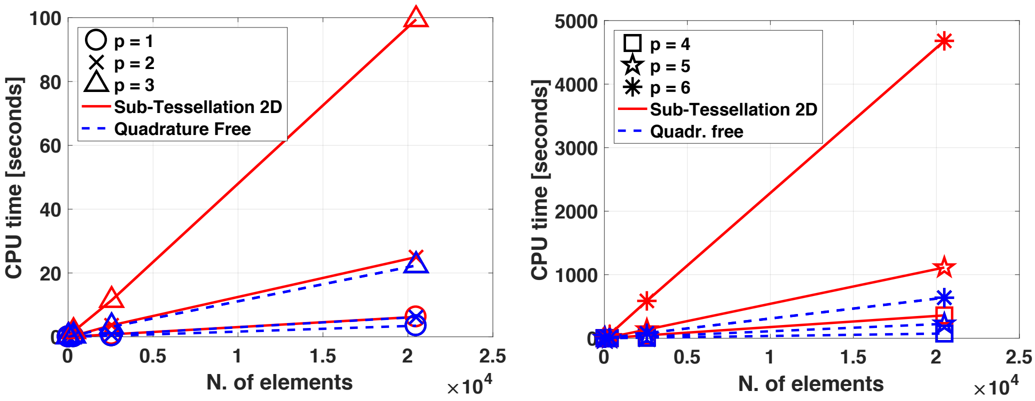

(a) Comparison for $p \in \{1, 2, 3\}$.
(b) Comparison for $p \in \{4, 5, 6\}$.

Figure 14: Comparison of the CPU time needed to assemble the global matrices $\mathbf{S}$ and $\mathbf{I}$ for a three–dimensional problem by using the proposed *Quadrature Free Method* and the classical *Sub-Tessellation* method. For each approach, each line is obtained by fixing the polynomial approximation degree $p \in \{1, 2, 3\}$ (left) and $p \in \{4, 5, 6\}$ (right), and measuring the CPU time by varying the number of elements of the underlying mesh.

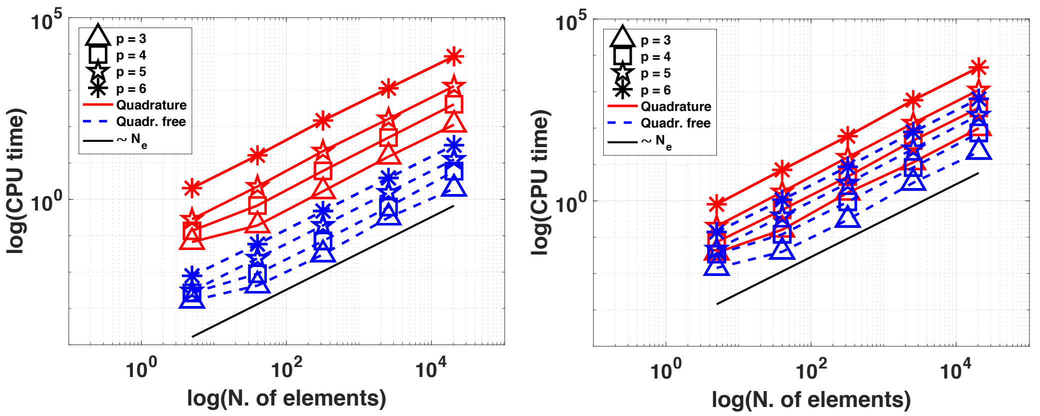

(a) CPU time comparison needed to assemble $\mathbf{M}$ and $\mathbf{V}$ in log-log scale.
(b) CPU time comparison needed to assemble $\mathbf{S}$ and $\mathbf{I}$ in log-log scale.

Figure 15: Comparison between the CPU time needed by the two method to assemble the global matrices $\mathbf{M}$ and $\mathbf{V}$ (left) and $\mathbf{S}$ and $\mathbf{I}$ (right) for a three–dimensional problem, versus the number of elements and for different choices of $p = 3, \ldots, 6$ (log-log scale).

Tessellation method both for volume and face integrals, although in this particular case no sub-tessellation is required for the face integrals, since they simply consist of triangular domains. Moreover, as in this case a sub-tessellation into tetrahedral domains is already given by the definition of the polyhedral mesh, the *Gaussian Quadrature Integration* for volume integrals on a general agglomerated polyhedral element $\kappa = \cup_{\kappa'_f \in \mathscr{S}_\kappa} \kappa'_f$ is realized by applying an exact *Gaussian quadrature* rule on each tetrahedron $\kappa'_f \in \mathscr{S}_\kappa$. The comparison of the CPU times for the two methods outlined here are presented for a set of agglomerated polyhedral grids where we vary the number of elements $N_e \in \{5, 40, 320, 2560, 20480\}$, and the polynomial degree $p \in \{1, 2, 3, 4, 5, 6\}$. For each agglomerated polyhedral grid $\mathcal{T}_h$ we have chosen the corresponding fine tetrahedral grid $\mathcal{T}_{fine}$ such that the cardinality of the set $\mathscr{S}_\kappa$ appearing in (33) is $|\mathscr{S}_\kappa| \sim 10\ \forall \kappa \in \mathcal{T}_h$. The results are shown in Figure 13 for the computation of the matrices $\mathbf{M}$ and $\mathbf{V}$, and in Figure 14 for the computation of matrices $\mathbf{S}$ and $\mathbf{I}$. Here, we observe analogous behaviour to the two–dimensional case: the *Quadrature Free Method* substantially outperforms the *Gaussian Quadrature Integration* both for the computation of the volume and face integrals. We also have reported in Figure 15 the logarithmic-scaled graphs of each computation, showing that, as expected, the gain in terms of CPU time given by the use of the proposed method is more evident here, with respect of two–dimensional case, also for the face integrals.

Conclusions

We have proposed a new approach for the numerical evaluation of the integrals required to assemble the mass and stiffness matrices arising from the DG discretization of diffusion-reaction problems, where the underlying mesh is composed by polygonal/polyhedral elements. Starting from the idea proposed in [26] for the integration of *homogeneous functions*, we have developed a cubature method which does not require the definition of a set of nodes and weights on the domain of integration, and allows for the exact integration of polynomial functions based on evaluating the integrand only at the vertices of the polytopal integration domain. This approach shows a remarkable gain in terms of CPU time with respect to classical quadrature rules, maintaining the same degree of accuracy. On the one hand, the number of computations is optimized, with respect to the polynomial degree of the integrand, and moreover less memory storage is required as no sub-partition and quadrature nodes and weights are required. With regards the three–dimensional tests presented Section 5.2, we note that more substantial gains in terms of CPU time, with respect to classical approaches, can be obtained if the underlying grid is composed of pure (not agglomerated) polyhedral elements: firstly, this is because a sub-partition should be defined on the fly for each element, and secondly, as faces are not only triangles but possibly polygons of general shape, a sub-tessellation is needed also for surface integrals. The proposed technique is completely general and can be extended to several numerical methods based on discrete spaces defined on polygonal/polyhedral meshes, such as Virtual Element Method, Mimetic Finite Difference, Hybrid High-Order, Hybridizable Discontinuous Galerkin, Polygonal Finite Element Method, for example. We stress that for moderate polynomial degrees, the proposed integration technique, which involves exact integration of bivariate and trivariate functions in two- and three–dimensions, respectively, has been observed to be numerically stable.

References

[1] P. F. Antonietti, F. Brezzi, and L. D. Marini. Bubble stabilization of discontinuous Galerkin methods. *Comput. Methods Appl. Mech. Engrg.*, 198(21-26):1651–1659, 2009.

[2] P. F. Antonietti, A. Cangiani, J. Collis, Z. Dong, E. H. Georgoulis, S. Giani, and P. Houston. *Review of discontinuous Galerkin Finite Element Methods for partial differential equations on complicated domains*, volume 114 of *Lecture Notes in Computational Science and Engineering*, chapter 8, pages 281 – 310. Springer, 1st edition, 2016.

[3] P. F. Antonietti, L. Beirão da Veiga, D. Mora, and M. Verani. A stream Virtual Element formulation of the Stokes problem on polygonal meshes. *SIAM J. Numer. Anal.*, 52(1):386 – 404, 2014.

[4] P. F. Antonietti, L. Beirão da Veiga, S. Scacchi, and M. Verani. A C1 Virtual Element Method for the Cahn-Hilliard equation with polygonal meshes. *SIAM J. Numer. Anal.*, 54(1):34 – 56, 2016.

[5] P. F. Antonietti, C. Facciolà, A. Russo, and M. Verani. Discontinuous Galerkin approximation of flows in fractured porous media. *Technical Report 22/2016, MOX Report*, 2016.

[6] P. F. Antonietti, L. Formaggia, A. Scotti, M. Verani, and N. Verzotti. Mimetic Finite Difference approximation of flows in fractured porous media. *ESAIM Math. Model. Numer. Anal.*, 50(3):809 – 832, 2016.

[7] P. F. Antonietti, S. Giani, and P. Houston. *hp*-version Composite Discontinuous Galerkin methods for elliptic problems on complicated domains. *SIAM J. Sci. Comput.*, 35(3):A1417 – A1439, 2013.

[8] P. F. Antonietti, S. Giani, and P. Houston. Domain decomposition preconditioners for discontinuous Galerkin methods for elliptic problems on complicated domains. *J. Sci. Comput.*, 60(1):203–227, 2014.

[9] P. F. Antonietti, G. Manzini, and M. Verani. The fully nonconforming Virtual Element Method for biharmonic problems. *Math. Mod. Meth. Appl. Sci.*, Accepted: 16 October 2017.

[10] P. F. Antonietti and G. Pennesi. V-cycle multigrid algorithms for discontinuous Galerkin methods on non-nested polytopic meshes. *MOX Report No. 49/2017*, submitted 2017.

[11] N. D. Arnold, F. Brezzi, B. Cockburn, and L. D. Marini. Unified analysis of discontinuous Galerkin methods for elliptic problems. *SIAM J. Numer. Anal.*, 39(5):1749 – 1779, 2001/2002.

[12] B. Ayuso de Dios, K. Lipnikov, and G. Manzini. The nonconforming Virtual Element Method. *ESAIM Math. Model. Numer. Anal.*, 50(3):879 – 904, 2016.

[13] F. Bassi, L. Botti, and A. Colombo. Agglomeration-based physical frame dG discretizations: an attempt to be mesh free. *Math. Mod. Meth. Appl. Sci.*, 24(8):1495–1539, 2014.

[14] L. Beirão da Veiga, F. Brezzi, A. Cangiani, G. Manzini, L. D. Marini, and A. Russo. Basic principles of Virtual Element Methods. *Math. Models Methods Appl. Sci.*, 23(1):199 – 214, 2013.

[15] L. Beirão da Veiga, F. Brezzi, L. D. Marini, and A. Russo. Mixed Virtual Element Methods for general second order elliptic problems on polygonal meshes. *ESAIM Math. Model. Numer. Anal.*, 50(3):727 – 747, 2016.

[16] L. Beirão da Veiga, F. Brezzi, L. D. Marini, and A. Russo. Virtual Element Method for general second-order elliptic problems on polygonal meshes. *Math. Models Methods Appl. Sci.*, 26(4):729 – 750, 2016.

[17] L. Beirão da Veiga, K. Lipnikov, and G. Manzini. *The Mimetic Finite Difference method for elliptic problems*, volume 11. Springer, Cham, 2014.

[18] F. Brezzi, K. Lipnikov, and M. Shashkov. Convergence of the Mimetic Finite Difference method for diffusion problems on polyhedral meshes. *SIAM J. Numer. Anal.*, 43(5):1872 – 1896 (electronic), 2005.

[19] F. Brezzi, K. Lipnikov, and M. Shashkov. Convergence of Mimetic Finite Difference method for diffusion problems on polyhedral meshes with curved faces. *Math. Mod. Meth. Appl. Sci.*, 16(2):275 – 297, 2006.

[20] F. Brezzi, K. Lipnikov, and V. Simoncini. A family of Mimetic Finite Difference methods on polygonal and polyhedral meshes. *Math. Mod. Meth. Appl. S.*, 15(10):1533 – 1551, 2005.

[21] A. Cangiani, Z. Dong, and E. H. Georgoulis. *hp*-Version space-time discontinuous Galerkin methods for parabolic problems on prismatic meshes. *SIAM J. Sci. Comput.*, 39(4):A1251 – A1279, 2017.

[22] A. Cangiani, Z. Dong, E. H. Georgoulis, and P. Houston. *hp*-Version discontinuous Galerkin methods for advection-diffusion-reaction problems on polytopic meshes. *ESAIM Math. Model. Numer. Anal.*, 50:699 – 725, 2016.

[23] A. Cangiani, Z. Dong, E. H. Georgoulis, and P. Houston. *hp-Version discontinuous Galerkin methods on polygonal and polyhedral meshes.* SpringerBriefs in Mathematics. Springer International Publishing, 2017.

[24] A. Cangiani, E. H. Georgoulis, and P. Houston. *hp*-Version discontinuous Galerkin methods on polygonal and polyhedral meshes. *Math. Models Methods Appl. Sci.*, 24(10):2009 – 2041, 2014.

[25] A. Cangiani, G. Manzini, and O. J. Sutton. Conforming and nonconforming Virtual Element Methods for elliptic problems. *IMA J. Numer. Anal.*, 37(3):1317 – 1354, 2017.

[26] E. B. Chin, J. B. Lasserre, and N. Sukumar. Numerical integration of homogeneous functions on convex and nonconvex polygons and polyhedra. *Comput. Mech.*, 56(6):967 – 981, 2015.

[27] E. B. Chin, J. B. Lasserre, and N. Sukumar. Modeling crack discontinuities without element-partitioning in the extended finite element method. *Internat. J. Numer. Methods Engrg.*, 110(11):1021 – 1048, 2017.

[28] B. Cockburn, B. Dond, and J. Guzmán. A superconvergent LDG-hybridizable Galerkin method for second-order elliptic problems. *Math. Comp.*, 77(264):1887–1916, 2008.

[29] B. Cockburn, J. Gopalakrishnan, and R. Lazarov. Unified hybridization of discontinuous Galerkin, mixed, and continuous Galerkin methods for second order elliptic problems. *SIAM J. Numer. Anal.*, 47(2):1319–1365, 2009.

[30] B. Cockburn, J. Gopalakrishnan, and F.-J. Sayas. A projection-based error analysis of HDG methods. *Math. Comp.*, 79(271):1351–1367, 2010.

[31] B. Cockburn, J. Guzmán, and H. Wang. Superconvergent discontinuous Galerkin methods for second-order elliptic problems. *Math. Comp.*, 78(265):1–24, 2009.

[32] D. A. Di Pietro and A. Ern. A Hybrid High-Order locking-free method for linear elasticity on general meshes. *Comput. Methods Appl. Mech. Engrg.*, 283(1):1 – 21, 2015.

[33] D. A. Di Pietro and A. Ern. Hybrid High-Order methods for variable-diffusion problems on general meshes. *C. R. Math. Acad. Sci. Soc. R. Can.*, 353(1):31 – 34, January 2015.

[34] D. A. Di Pietro, A. Ern, and S. Lemaire. An arbitrary-order and compact-stencil discretization of diffusion on general meshes based on local reconstruction operators. *Comput. Method Appl. Math.*, 14(4):461 – 472, October 2014.

[35] J. Droniou, R. Eymard, and R. Herbin. Gradient schemes: generic tools for the numerical analysis of diffusion equations. *ESAIM Math. Model. Numer. Anal.*, 50(3):749 – 781, 2016.

[36] T.-P. Fries and T. Belytschko. The extended/generalized finite element method: an overview of the method and its applications. *Internat. J. Numer. Methods Engrg.*, 84(3):253–304, 2010.

[37] A. Gerstenberger and A. W. Wall. An Extended Finite Element Method/Lagrange multiplier based approach for fluid-structure interaction. *Comput. Methods Appl. Mech. Engrg.*, 197(19 - 20):1699 – 1714, 2008.

[38] S. Giani and P. Houston. Domain decomposition preconditioners for discontinuous Galerkin discretizations of compressible fluid flows. *Numer. Math. Theory Methods Appl.*, 7(2):123 – 148, 2014.

[39] D. J. Griffiths. *Introduction to Quantum Mechanics.* Pearson Education, 2005.

[40] W. Hackbusch and S. A. Sauter. Composite Finite Elements for problems containing small geometric details. Part II: Implementation and numerical results. *Comput. Visual Sci.*, 1(4):15–25, 1997.

[41] W. Hackbusch and S. A. Sauter. Composite Finite Elements for the approximation of PDEs on domains with complicated micro-structures. *Numer. Math.*, 75(4):447–472, 1997.

[42] D. J. Holdych, D. R. Noble, and R. B. Secor. Quadrature rules for triangular and tetrahedral elements with generalized functions. *Internat. J. Numer. Methods Engrg.*, 73(9):1310 – 1327, 2015.

[43] J. Hyman, M. Shashkov, and S. Steinberg. The numerical solution of diffusion problems in strongly heterogeneous non-isotropic materials. *J. Comput. Phys.*, 132(1):130 – 148, 1997.

[44] G. Karypis and V. Kumar. A fast and high quality multilevel scheme for partitioning irregular graphs. *SIAM J. Sci. Comput.*, 20(1):359 – 392, 1998.

[45] G. Karypis and V. Kumar. Metis: Unstructured graph partitioning and sparse matrix ordering system, version 4.0. `http://www.cs.umn.edu/~metis`, 2009.

[46] J. B. Lasserre. Integration on a convex polytope. *Proc. Amer. Math. Soc.*, 126(8):2433 – 2441, 1998.

[47] C.-J. Li, P. Lambertu, and C. Dagnino. Numerical integration over polygons using an eight-node quadrilateral spline finite element. *J. Comput. Appl. Math.*, 233(2):279 – 292, 2009.

[48] J. N. Lyness and G. Monegato. Quadrature rules for regions having regular hexagonal symmetry. *SIAM J. Numer. Anal.*, 14(2):283 – 295, 1977.

[49] J. Ma, V. Rokhlin, and S. Wandzura. Generalized Gaussian quadrature of systems of arbitrary functions. *SIAM J. Numer. Anal.*, 33(3):971 – 996, 1996.

[50] N. Mo´es, J. Dolbow, and T. Belytschko. A finite element method for crack growth without remeshing. *Int. J. Numer. Meth. Eng.*, 46(1):131 – 150, 1999.

[51] S. E. Mousavi and N. Sukumar. Numerical integration of polynomials and discontinuous functions on irregular convex polygons and polyhedrons. *Comput. Mech.*, 47(5):535 – 554, 2011.

[52] S. E. Mousavi, H. Xiao, and N. Sukumar. Generalized Gaussian quadrature rules on arbitrary polygons. *Internat. J. Numer. Methods Engrg.*, 82(1):99 – 113, 2010.

[53] S. Natarajan, S. Bordas, and D. R. Mahapatra. Numerical integration over arbitrary polygonal domains based on Schwarz–Christoffel conformal mapping. *Internat. J. Numer. Methods Engrg.*, 80(1):103 – 134, 2009.

[54] A. Quarteroni, R. Sacco, and F. Saleri. *Numerical Mathematics.* Springer, 2007.

[55] C. P. Simon and L. E. Blume. *Mathematics for Economists.* W. W. Norton and Company: New York, 1996.

[56] A. Sommariva and M. Vianello. Product Gauss cubature over polygons based on Green's integration formula. *BIT*, 47(2):441 – 453, 2007.

[57] A. H. Stroud and D. Secrest. Gaussiam quadrature formulas. *ZAMM Z. Angew. Math. Mech.*, 47(2):138 – 139, 1967.

[58] Y. Sudhakar and W. A. Wall. Quadrature schemes for arbitrary convex/concave volumes and integration of weak form in enriched partition of unity methods. *Comput. Methods Appl. Mech. Engrg.*, 258(1):39 – 54, 2013.

[59] N. Sukumar, N. Mo´es, and T. Belytschko. Extended Finite Element Method for three-dimensional crack modelling. *Internat. J. Numer. Methods Engrg.*, 48(11):1549 – 1570, August 2000.

[60] N. Sukumar and A. Tabarraei. Conforming Polygonal Finite Elements. *Internat. J. Numer. Methods Engrg.*, 61(12):2045–2066, 2004.

[61] A. Tabarraei and N. Sukumar. Extended Finite Element Method on polygonal and quadtree meshes. *Comput. Methods Appl. Mech. Eng.*, 197(5):425–438, 2008.

[62] C. Talischi, G. H. Paulino, A. Pereira, and I. F. M. Menezes. Polymesher: A general-purpose mesh generator for polygonal elements written in matlab. *Struct. Multidiscip. Optim.*, 45(3):309–328, 2012.

[63] M. E. Taylor. *Partial Differential Equations: Basic Theory.* Springer-Verlag, New york, 1996.

[64] G. Ventura. On the elimination of quadrature subcells for discontinuous functions in the extended finite-element method. *Internat. J. Numer. Methods Engrg.*, 66(5):761 – 795, 2006.

[65] G. Ventura and E. Benvenuti. Equivalent polynomials for quadrature in Heaviside function enriched elements. *Internat. J. Numer. Methods Engrg.*, 102(3 - 4):688 – 710, 2015.

[66] H. Xiao and Z. Gimbutas. A numerical algorithm for the construction of efficient quadrature rules in two and higher dimensions. *Comput. Math. Appl.*, 59(2):663 – 676, January 2010.

[67] N. Yarvin and V. Rokhlin. Generalized Gaussian quadratures and singular value decompositions of integral operators. *SIAM J. Sci. Comput.*, 20(2):669 – 718, 1998.

[68] A. M. Yogitha and K. T. Shivaram. Numerical integration of arbitrary functions over a convex and non convex polygonal domain by eight noded linear quadrilateral finite element method. *Aust. J. Basic Appl. Sci.*, 10(16):104 – 110, 2016.

MOX Technical Reports, last issues

Dipartimento di Matematica
Politecnico di Milano, Via Bonardi 9 - 20133 Milano (Italy)

02/2018 Canuto, C.; Nochetto, R. H.; Stevenson, R.; Verani, M.
A saturation property for the spectral-Galerkin approximation of a Dirichlet problem in a square

01/2018 Berrone, S.; Bonito, A.; Stevenson, R.; Verani, M.
An optimal adaptive Fictitious Domain Method

67/2017 Esterhazy, S.; Schneider, F.; Mazzieri, I; Bokelmann, G.
Insights into the modeling of seismic waves for the detection of underground cavities

68/2017 Paolucci, R.; Infantino, M.; Mazzieri, I.; Özcebe, A.G.; Smerzini, C.; Stupazzini, M.
3D physics-based numerical simulations: advantages and current limitations of a new frontier to earthquake ground motion prediction. The Istanbul case study.

66/2017 Tamellini, M.; Parolini, N.; Verani, M.
An optimal control problem of two-phase compressible-incompressible flows

64/2017 Fumagalli, I.; Parolini, N.; Verani, M.
Optimal control in ink-jet printing via instantaneous control

65/2017 Regazzoni, F.;Parolini, N.;Verani M.
Topology optimization of multiple anisotropic materials, with application to self-assembling diblock copolymers

62/2017 Barbarotta, L.; Rossi, S.; Dede', L.; Quarteroni, A.
A Transmurally Heterogeneous Orthotropic Activation Model for Ventricular Contraction and its Numerical Validation

63/2017 Masci, C.; Paganoni, A.M.; Ieva, F.
Non-parametric mixed-effects models for unsupervised classification of Italian schools

61/2017 Vadacca, L.; Colciago, C. M.; Micheletti, S.; Scotti, A.
Three-dimensional fault representation by interface and solid elements: effects of the anisotropy of the fault zone permeability on the timing of triggered earthquakes